2649-1-F
Copy____
Volume 1

THE UNIVERSITY OF MICHIGAN

COLLEGE OF ENGINEERING

DEPARTMENT OF ELECTRICAL ENGINEERING

Radiation Laboratory

ANALYSIS OF ARIS DATA

Final Report (1 December 1969 - 1 July 1970) : Volume 1

By

Eugene F. Knott and Thomas B. A. Senior

July 1970

Contract F 08606-69-C-0045

Contract with

Air Force Eastern Test Range

ARIS Ships Re-entry Division

Patrick Air Force Base, Florida 32925

Ann Arbor, Michigan

FOREWORD

This report is the second and final document submitted to the Air Force Eastern Test Range, ARIS Reentry Ships Division, Patrick Air Force Base, Florida 32925 under Contract F08606-69-C-0045. Four similar documents were submitted under a previous contract (F08606-67-C-0071) and this final report is essentially the sixth of a related series. This report is printed in two volumes.

The research was performed by members of the Radiation Laboratory of The University of Michigan, Department of Electrical Engineering and administered by Prof. Ralph E. Hiatt, Head of the Radiation Laboratory. Mr. Eugene F. Knott was the Principal Investigator and Prof. Thomas B. A. Senior guided the electromagnetic scattering studies during this reporting period.

The detailed research reported herein covers the period 1 December 1969 through 1 July 1970 and a brief summary is included that covers the period from 15 April 1967 to 1 July 1970.

ACKNOWLEDGEMENT

The authors are grateful to Dr. P. L. E. Uslenghi for his work on disk scattering and to Mr. Chester Grabowski for his cone measurements. Other contributors were Dr. William Parker and Mr. Walter Linck in programming, and Mrs. Claire White and Mrs. Mary Wright in the inevitable clerical details.

ABSTRACT

Unclassified

In Volume 1 of this Final Report, we firstly touch on the major contributions made during the 38-month span of two successive contracts, which to all intents address a single goal: to assess the data and data collection techniques of the Advanced Range Instrumentation Ships, and to recommend how improvements could be made. The technical details of the report commence with a description of a final laboratory test of the five-parameter method conceived and described in the preceding report. The test suggested that polarization angle history can be a potential source of aspect angle information and this possibility is examined for the case of circular polarization. A summary of extensive theoretical and experimental work on cone and disk scattering is given, showing how the disk results contributed to the more practical case of the cone. We conclude with a recommendation that the five-parameter method be seriously considered for instrumentation.

In Volume 2 of this Final Report, we present a sequence of three related test support missions and a comparison shows that differences as well as similarities exist.

TABLE OF CONTENTS

LIST OF ILLUSTRATIONS (U)

This Chapter is UNCLASSIFIED

I

SUMMARY OF RESEARCH

1.1 Introduction

This final report concludes approximately 38 months of research performed under Air Force contracts F08606-67-C-0071 and F8608-69-C-0045. It is the sixth of a series issued at approximately six-month intervals and the second issued under the present contract. The contents of all six documents are given in Appendix A.

This report is divided into six chapters, of which only Chapter IV is classified, and two appendices. In Section 1.2 of this, the first, chapter we list the major accomplishments of the research performed over the last three years, and point out that many of the results are also applicable to sensors other than ARIS which possess the multiple polarization capabilities that ARIS enjoys.

Chapter II describes a final laboratory test of the five-parameter method which was undertaken because of an experimental anomaly that was discovered in the previous tests. Chapter III examines the relation between true body polarization angle and true body aspect angle, and should prove to be highly useful if the five-parameter scheme is instrumented.

Chapter IV is a survey of the results of a group of three related Test Support missions, one of which was analyzed in the previous report. Chapter V summarizes the results of a theoretical and experimental study of disk and cone scattering, part of which had been undertaken early in the first contract. Chapter VI is a very brief collection of conclusions and recommendations for further study.

Appendix A lists the contents of the formal reports submitted to ETR since the first contract was awarded in April of 1967, and is useful in pinpointing specific areas of effort. Appendix B contains a collection of radar cross section charts that we have found useful in signature analysis.

1.2 Summary of Research

The goal of the research has been to discover ways in which the collection and processing of ARIS data could be improved and throughout the contract period we have taken a radar data user's viewpoint to do so. The emphasis has been on radar signatures, as opposed to metric data, because the radar data can lead to refined estimates of target size and shape when in most instances the metric data reveal only gross characteristics.

By adopting the viewpoint of a user of radar signature data we isolated many of the problems that besiege the analyst and developed analytical methods that can expedite his task. Some of the problems involve data accuracy and others involve data processing; some of the methods use existing data while others assume the possibility of acquiring data not yet available. Examples of our accomplishments are highlighted in the areas presented below and although our purpose was to explore and define improvements to the ARIS system, many of the applications reach far beyond ARIS. Indeed, most of the concepts are applicable to any sensor that possesses multiple polarization capability, whether it be linear or circular.

Metric Data

Although the major task was to work intensively with radar signature data, metric data are the source of the angular positions of major signature features such as lobes and nulls. Typical aspect angle plots often displayed improbable behavior and since these data are crucial to accurate analysis, we commenced a critical examination of aspect angle data. We found that the altitude dependence of the atmospheric index of refraction was often based upon a single low altitude measurement which in itself is not a severe criticism. But if the range is great enough, an imperfect atmospheric profile produces a virtual target position that is quite different from its true position. In another instance we found that arc-cosine functions were being used in the data reduction process when, in fact, arc-tangent functions could be used with improved accuracy. This is especially true

for small aspect angles, where errors in the metric rate data can have their largest effect. As a consequence of these investigations, the data processing was modified and aspect angle behavior has taken on more credibility.

Specific Test Analyses

Having undertaken detailed analyses of several tests, we have found that those in which the body is seen at large aspect angles are by far the easiest to analyze. As a result we developed procedures applicable to wide angle data with a high probability of success with but a small investment of labor. On the other hand, those tests in which the aspect angles remain small represent a much greater challenge and no completely successful technique exists. It is precisely because of these difficulties that we developed the two analytical methods cited below; one can be used to interpret data such as that currently available from ARIS, and the other will be useful if a modest change can be made in the instrumentation. It is significant that methods such as these evolve only from constant efforts to understand the data of specific test flights.

Cross Polarized Sizing

The advantages of the multiple polarization capacity of sensors such as ARIS is that each channel contains some information. The direct HH and VV returns have always been of more interest than the cross polarized VH and HV returns because they completely dominate the target scattering in the region of specular viewing angles. The case is quite different, however, for aspect angles in the nose-on region where specular returns are seldom seen; here the cross polarized returns take on new significance. In a study program aimed at understanding the nature of these echoes we found ample theoretical and experimental basis for the development of a cross polarized sizing method. Although a stringent application of it requires that several conditions be met, it can still be a very powerful tool even under relaxed conditions. In a few seconds, for example, a lower

bound can be established for the size of the body being studied, especially if seen in the nose-on region. This method, it should be noted, is but a single example of our efforts to make maximum use of the current ARIS configuration.

The Five-Parameter Method

In looking forward to future needs a natural question to ask is "What additional data are desirable?" The answer is that phase data are needed in order to completely determine the body's polarization scattering matrix, from which there is a high probability the body's principal plane scattering pattern could be recovered. This can be accomplished with a coherent multiple-polarization radar, but experience (as well as theory) shows that such a radar is feasible only for targets whose velocities are accurately known. This is because the phase angles due to the target's range completely mask those due to its orientation. Under most conditions, however, the amplitude and phase of the two cross polarized returns are equal. The relative phase between the HH and VV returns (the main diagonals of the scattering matrix) can thus be established by means of an intermediate reference to the phase of the cross polarized returns, with the result that the range dependence of the phase measurements disappears and the desired orientation dependence survives. The measurement scheme requires scarcely more than a phase detector bridging the horizontal and vertical receiving channels and represents an entirely feasible tradeoff between the advantages and disadvantages of a fully coherent radar.

Theoretical and Experimental Simulations

It is clear that one of the steps required for successful signature analysis is to recover significant portions of a target's principal plane scattering patterns. One must be able to relate such patterns to the size and shape of the target, which implies that in some measure one must be able to proceed in the more classical direction, (i.e., to predict the pattern of a known target). Body motion can easily

be synthesized along any trajectory, thus simulating true aspect angle history, but from this point on the simulation of signature data hinges on the dependability of theoretical scattering predictions. Realizing that scattering theory is not always as dependable as is desired we undertook two parallel paths: one was the construction of a mechanical motion simulator that reproduces, in a dynamic laboratory measurement environment, a large variety of body motions and the other was an independent upgrading of the state of the theory for bodies such as right circular cones. The mechanical simulator was highly successful (and very likely the only of its kind) and within a few months the necessary elements of an improved theoretical description were in hand.

This Chapter is UNCLASSIFIED

II

THE FIVE-PARAMETER SIZING; A SEQUEL

In our last report (the first interim engineering report under this contract, 2649-1-T) we suggested how the acquisition of a pair of phase differences in addition to the amplitude data (radar cross section) already gathered by ARIS could lead to better estimates of target attitude and to the recovery of portions of the body's principal plane patterns. This configuration is conceptually very simple and requires only a single phase detector bridging the horizontal and vertical receiving channels; recording equipment is assumed to be available with which to store the history of the detector output signal.

Ideally, of course, a fully coherent radar would be desirable so that the relative phase angles of the body's polarization scattering matrix would be determined. This is the objective of the coherent scattering matrix radar built at the MITRE Corporation. The disadvantage of a fully coherent radar is that simple target translation produces a much greater phase change than the target body motion and the phase data often resemble noise. The operators of the MITRE radar used the system on orbiting satellites and it was extremely important that the body trajectory and velocity be known in advance. We doubt that such a radar will be useful for reentry targets for several years.

The phase angle of each element of the target scattering matrix is advanced (or retarded) by the target range rate and the range must be known precisely in order that its influence on the scattering matrix be accounted for. The five-parameter technique, on the other hand, automatically removes the range dependence because the method uses phase differences, not absolute phase. Since the range dependence of the phase of each element of the scattering matrix is precisely the same, the phase differences that survive are due entirely to target orientation.

Implementing the technique requires that the four combinations of horizontal and vertical, transmitted and received, polarizations be available. Three amplitudes are required (σ_{HH}, σ_{VV}, and σ_{VH} or σ_{HV}, all being radar cross sections) and two phase differences ($\left[\phi_{HH} - \phi_{HV}\right]$ and $\left[\phi_{VV} - \phi_{VH}\right]$). With these input data, it can be shown that the true target polarization angle can be computed from

$$\psi = \frac{1}{2} \arctan \left| \frac{2\sqrt{\sigma_{VH}}}{\sqrt{\sigma_{HH}}\, e^{j(\phi_{HH}-\phi_{HV})} - \sqrt{\sigma_{VV}}\, e^{j(\phi_{VV}-\phi_{VH})}} \right| . \qquad (2.1)$$

Although the bracketed term on the right involves complex numbers, the denominator should turn out to be purely real. When actual data are acquired, this probably will not be the case, and the extent to which the data do not conform to expectations may serve as a useful guide to calibration and to trouble-shooting problems in the system.

Since the true body polarization angle is presumably known by virtue of (2.1), its value can be used in the following expressions for the target's instantaneous horizontal and vertical principal plane returns:

$$\sigma_H = \left| \left(\frac{1+\cos 2\psi}{2\cos 2\psi}\right)\sqrt{\sigma_{HH}}\, e^{j(\phi_{HH}-\phi_{HV})} - \left(\frac{1-\cos 2\psi}{2\cos 2\psi}\right)\sqrt{\sigma_{VV}}\, e^{j(\phi_{VV}-\phi_{VH})} \right|^2 , \qquad (2.2)$$

$$\sigma_V = \left| \left(\frac{1+\cos 2\psi}{2\cos 2\psi}\right)\sqrt{\sigma_{VV}}\, e^{j(\phi_{VV}-\phi_{VH})} - \left(\frac{1-\cos 2\psi}{2\cos 2\psi}\right)\sqrt{\sigma_{HH}}\, e^{j(\phi_{HH}-\phi_{HV})} \right|^2 . \qquad (2.3)$$

When the process is performed on each successive set of data points in time, the instantaneous values (2.2) and (2.3) should trace out portions of the principal plane target patterns flashed toward the radar during the target motion.

Two tests of the method were performed in the laboratory and the details of the tests were reported in the previous interim report. In the first test, a right circular cone was swept uniformly in aspect angle from nose-on incidence to about 24° off nose-on, and during the sweep polarizations were chosen to simulate VV, HH and HV measurements as they might be made in a real-world environment. Both the phase and the amplitudes of the returns were measured and when the data were used to reconstruct the principal plane patterns, the agreement was very good.

The second test was performed on three roll symmetric targets with the added complexity that the target motion was not a simple sweep in aspect, but a uniform circular precession instead. This test was implemented with the aid of the mechanical motion simulator designed and constructed in 1968 and although the simulator did its job well, we were not content with the results. When the phase and amplitude data were used to reconstruct the principal plane patterns, they were fairly well (though not perfectly) reproduced, but the cross polarized patterns were in serious error.

The reason, we suspected, was the way the laboratory models were installed upon the motion simulator; it seemed that because the targets pivoted about a point lying a considerable distance from their axes of symmetry, the downward pitch component of the precession also caused the models to move forward (toward the radar). The five-parameter method implicitly assumes that targets of roll symmetry will gyrate about a center of mass located on the target axis, an altogether reasonable assumption. But since our radar had not been forewarned that this was not the case, the phase changes were interpreted in the wrong sense. A sketch of the troublesome geometry is shown in Fig. 2-1, reproduced from a previous report.

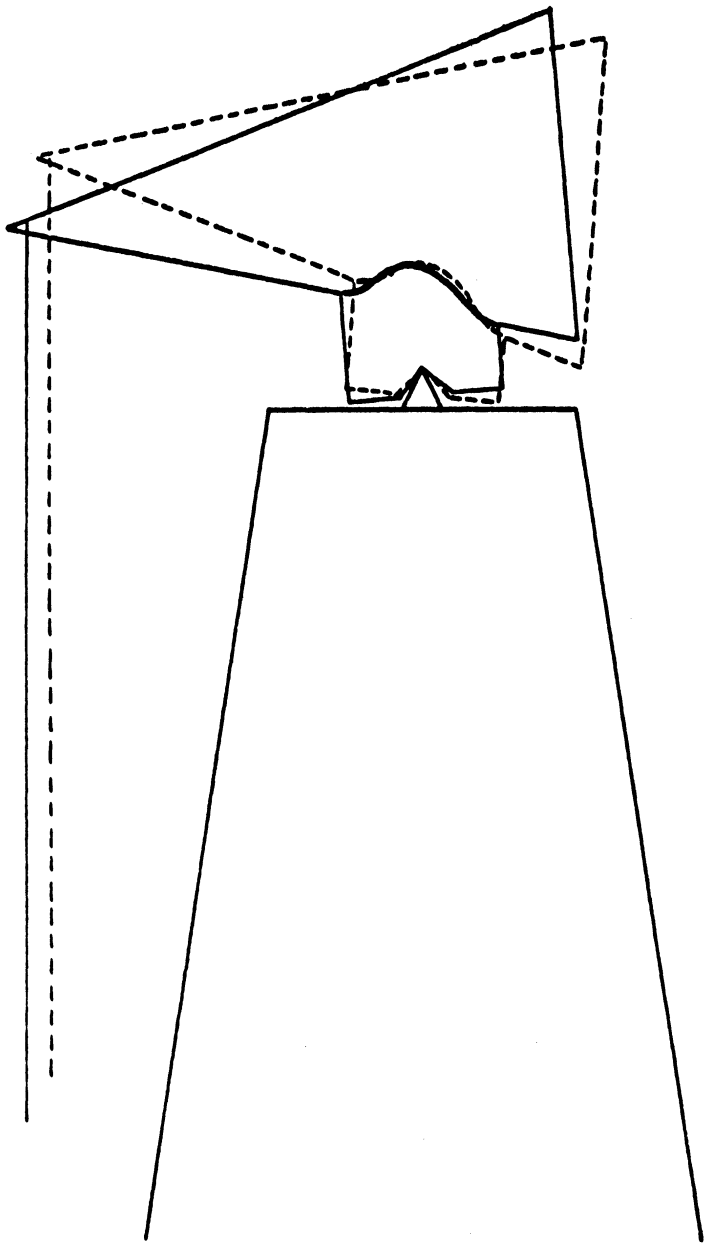

FIG. 2-1: Errors in the experiment are apparently due to the way we precessed the target. This side view shows that, because of the location of the pivot point, the target moves forward while it pitches down. Only the vertical component of the motion is affected; the horizontal component behaves normally.

The results suggested that a fairer test could be made if the target could be pivoted about a point on its axis. One way to do so is to construct an invisible yoke (made of dielectric material, for example) at the top of the column and fasten equally invisible support pins to the sides of the target that rest in the yoke. In practice, however, no feasible dielectric is invisible to the radar and these appendages will destroy the symmetry demanded of the target as well as produce interfering reflections. Instead of building such an arrangement we constructed a roll-symmetric target that could be supported very near its axis. The model is essentially a disk pierced by a rod and, as we shall presently see, its patterns in the nose-on region are similar to those of a cone. A sketch of the model is shown in Fig. 2-2.

As in previous tests, we selected appropriate polarization angles for the transmitting and receiving antennas and recorded simulated VV, HH and VH patterns while the target precessed through a circular path. The cone of precession had a half angle of 10^{o} and it was centered on a mean polarization angle of 30^{o} and mean aspect angle of 10^{o}. The phases of the returns were measured indirectly by use of a clever laboratory technique reported on in the previous interim report.

When the data were digitized, used in the inverted equations, and plotted on the principal plane patterns, the agreement was very good. Figures 2-3 and 2-4 show the comparison for the horizontal and vertical patterns and Fig. 2-5 shows the cross polarized pattern. Note that, because the precession cone half angle was 10^{o}, the maximum coverage of the reconstructed data was 20^{o}. The agreement was not as good for the cross polarized patterns probably because of the presence of experimental errors; note that the measured pattern (solid trace) is not symmetrical. Nonetheless, the cross polarized pattern reconstruction is a vast improvement over previous results and indicate that further experimental refinements would enhance the credibility of the method.

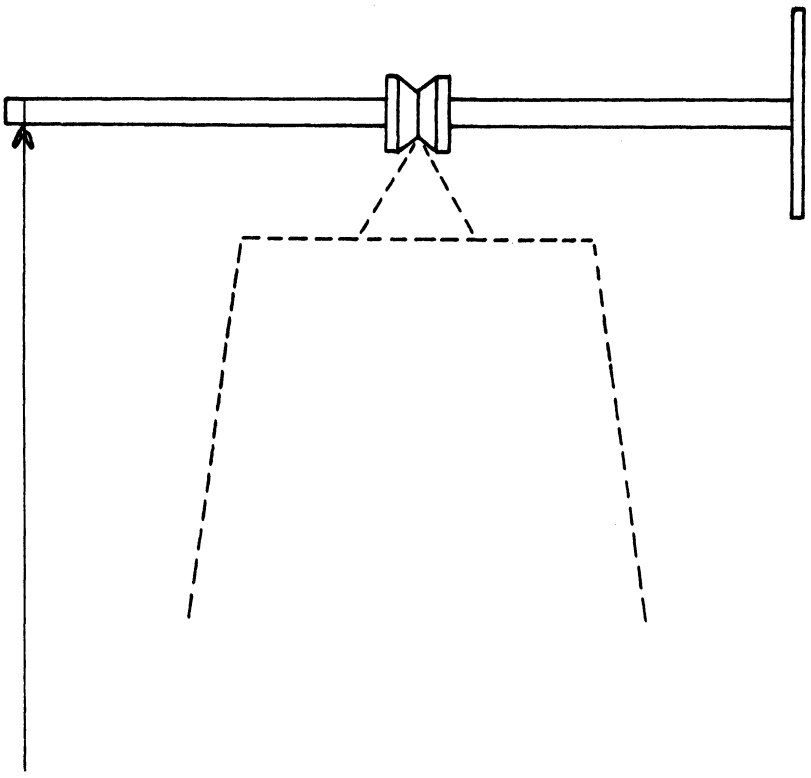

FIG. 2-2: This uncommon target satisfied the test requirements better than previous models: it is roll-symmetric and its axis lies close to the point of support. The metallic spool insures that the model will not slide off the styrofoam support wedge.

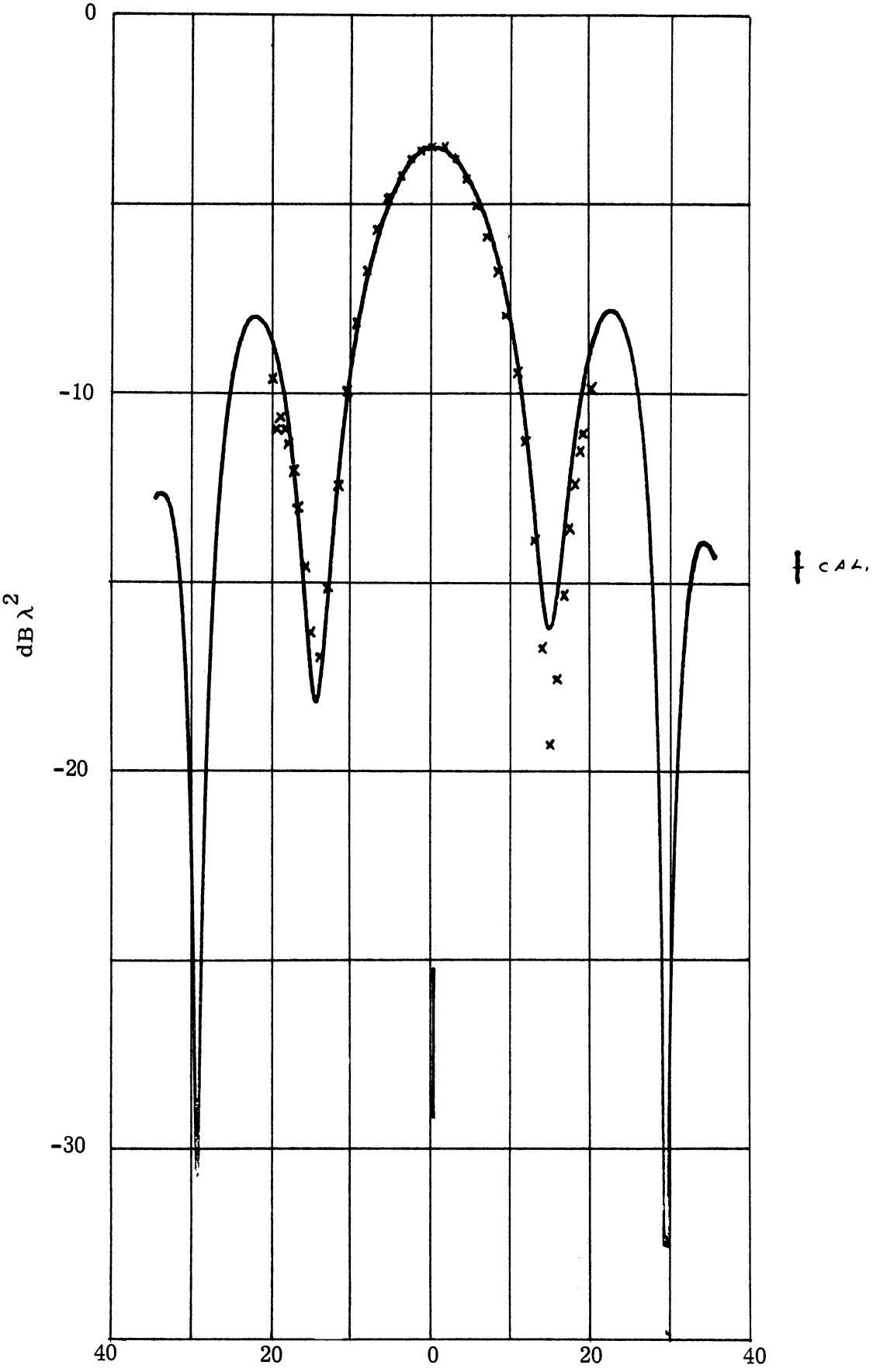

FIG. 2-3: Comparison of actual and reconstructed horizontal pattern.

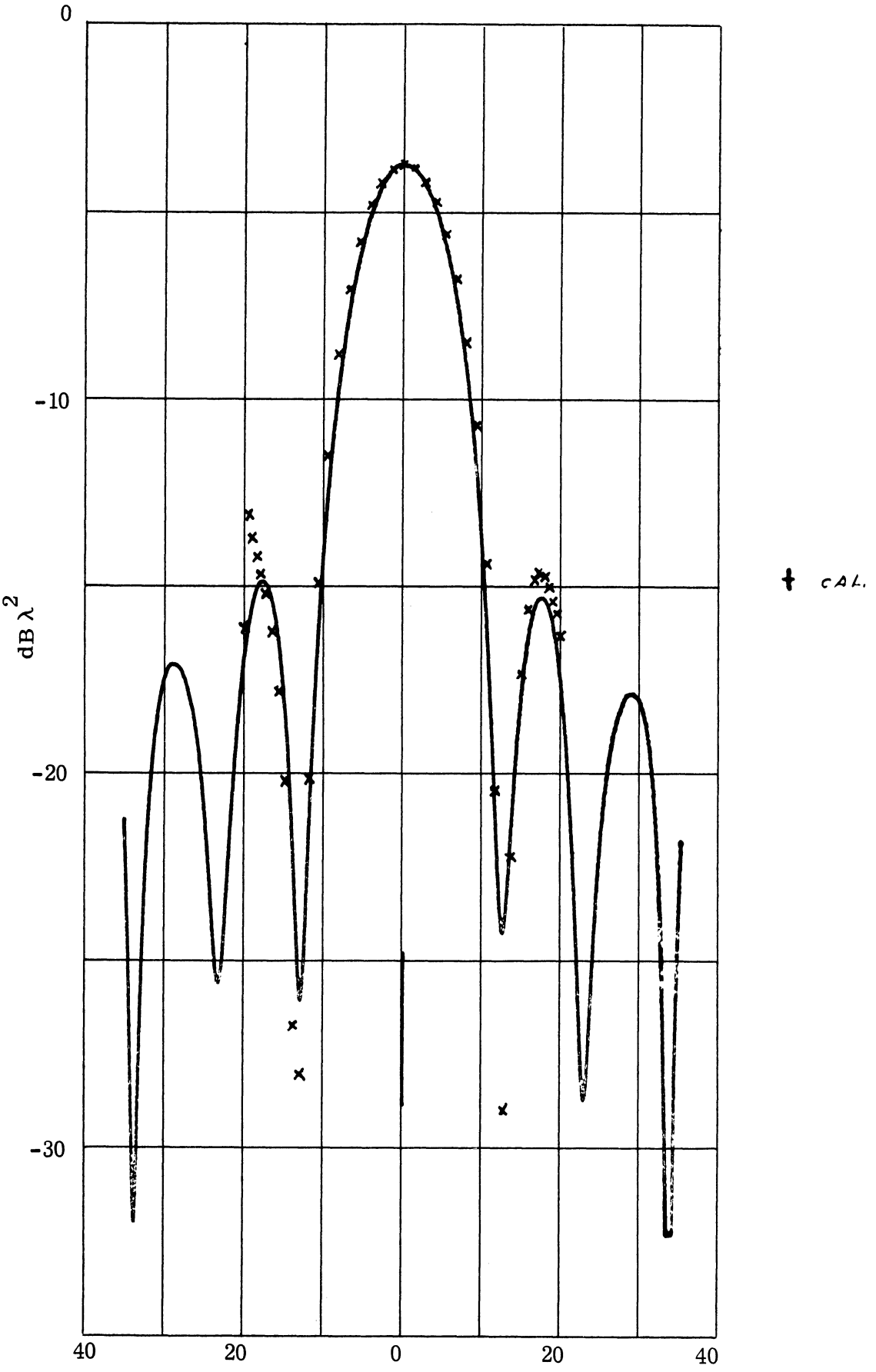

FIG. 2-4: Comparison of actual and reconstructed vertical pattern.

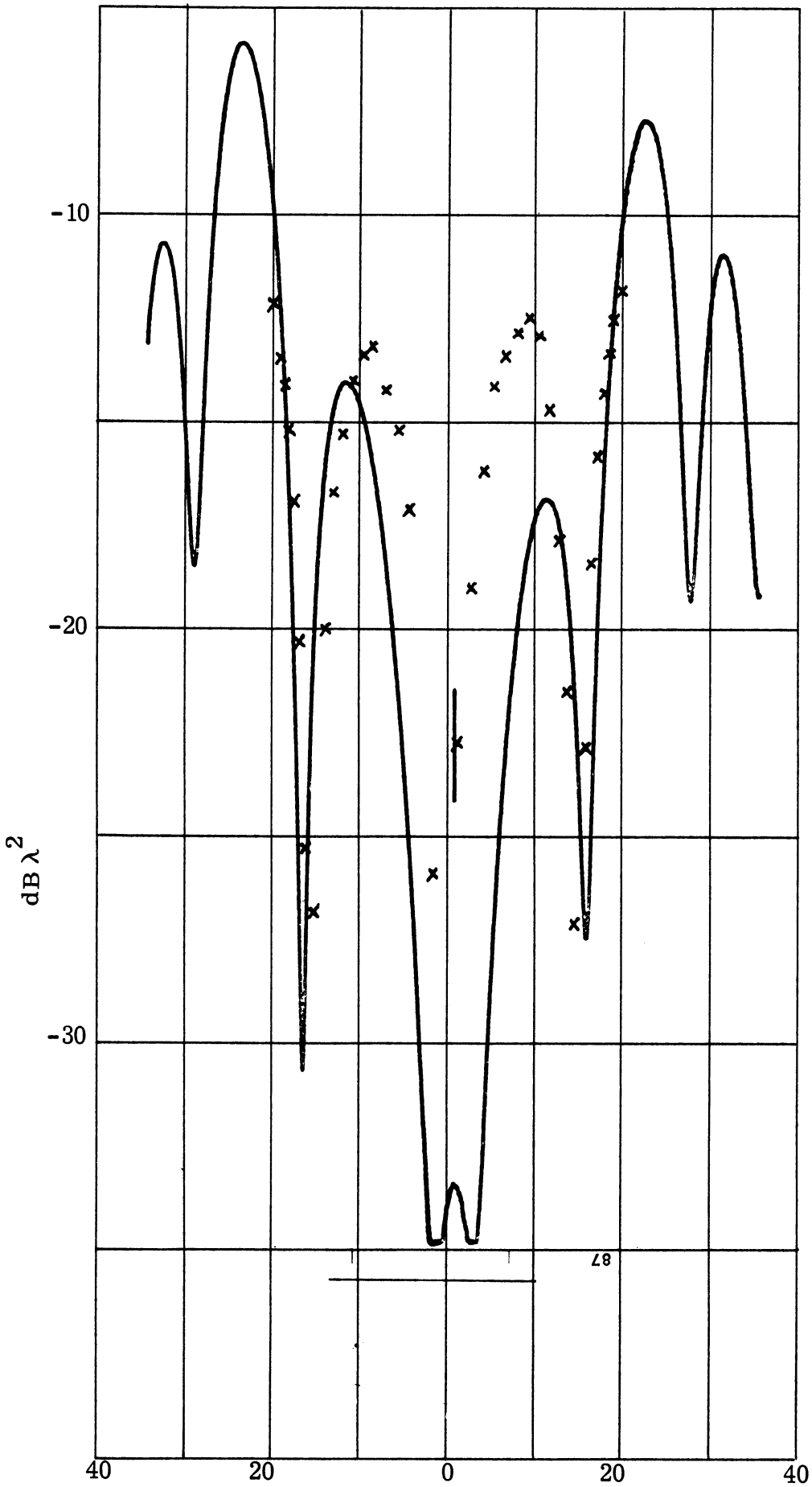

FIG. 2-5: Comparison of actual and reconstructed cross polarized pattern.

A final set of information provided by the five-parameter method is the polarization angle behavior during the motion simulation. The results plotted in Fig. 2-6 were disappointing at first, but this very plot generated the study presented in the next chapter. We were disheartened by the lack of any useful regularity in the results because it was known beforehand that the precession motion would sweep the polarization angle uniformly through a total of 180^{o}. It turns out the trouble can be traced to the complex nature of the argument in Eq. (2.1). In theory, the imaginary part vanishes, but in practice the data will naturally have enough error in them that a finite imaginary part remains. We took the obvious expedient of working with the absolute value of the argument, which automatically restricts the apparent polarization to the first quadrant($0 \leq \psi \leq \pi/2$) . A study of the errors steered us on to a new and far more important concept.

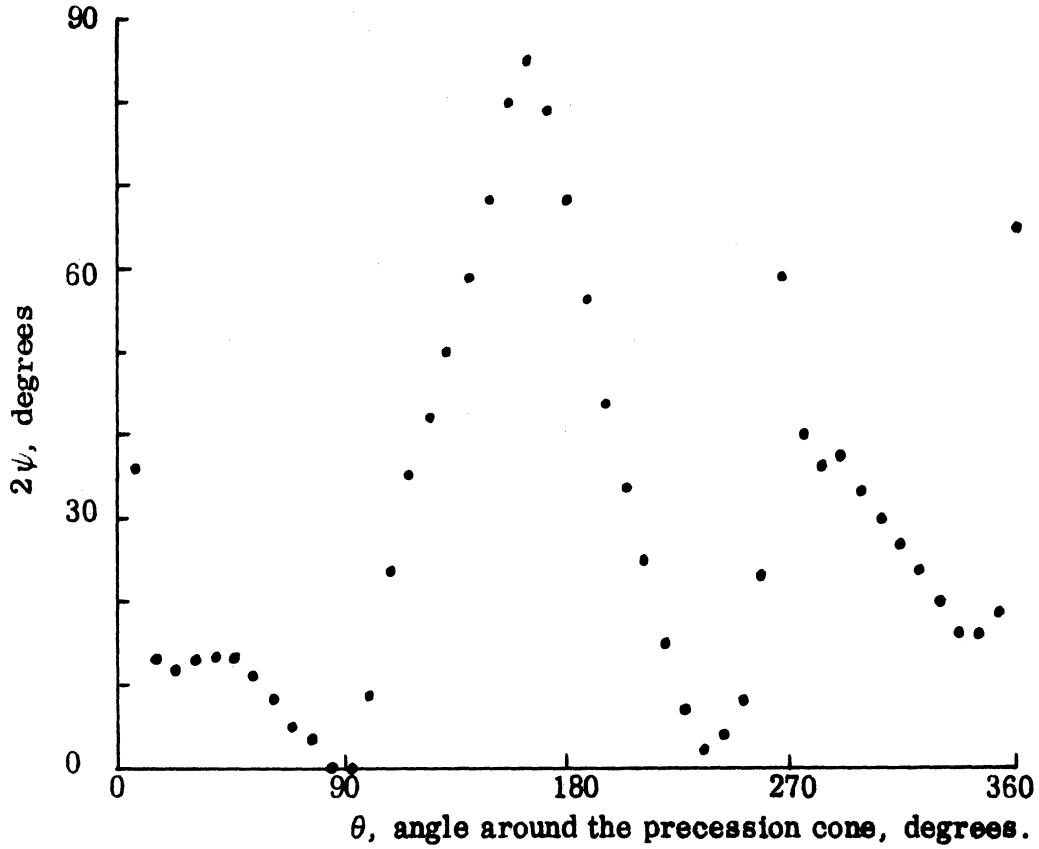

FIG. 2-6: This 'anomalous' behavior of the deduced polarization angle gave rise to the study of Chapter III; the anomalies are resolved there and a promising technique proposed.

This Chapter is UNCLASSIFIED

III

POLARIZATION AND ASPECT ANGLES

3.1 Introduction

The experimental testing of the five-parameter method in the laboratory has demonstrated that principal plane patterns of targets can be reconstructed from simulated signature data; moreover, the cross polarized patterns are available because of the quantity of information the method employs. It turns out, however, that unless aspect information is somehow available, the patterns cannot be related to viewing angles. The reconstructed patterns in Figs. 2-3 through 2-5 could be labelled with aspect angle because the motion was known; in a reentry environment this is not always true.

The anomolous behavior of the polarization angle of Fig. 2-6 was responsible for the development of a method of estimating true aspect angle based on polarization angle history and this will be described presently. The behavior is 'anomolous' because we know from the laboratory conditions that the polarization angle swept from -60^{o} to 120^{o}, yet the plotted data are constrained between 0^{o} and 90^{o} . This was the consequence of using the absolute value of the bracketed quantity in Eq. (2. 1); although the argument must theoretically be a pure real number, in practice it has an imaginary component due to experimental error. By working with the absolute value, we automatically confine the polarization angle to lie between 0^{o} and 90^{o} .

Although this is a problem that needs further study, we put it aside for a moment in order to become acquainted with a related problem: the behavior of the polarization angle for typical elliptical precession paths.

If the five-parameter method is instrumented, data will be acquired that have never before been available and it is well to be familiar with the typical behavior in advance. Although the behavior presented in Section 3.3 is idealized because of the absence of any real-world data to examine, it serves

to acquaint us with features that will probably be observed. To this end, we commenced the study explained in Section 3.2 below.

3.2 Effect of Elliptical Precession on True Aspect and Polarization Angles

A spinning body of roll symmetry executes elliptical precession in the presence of retarding reentry forces. A mathematical description of the motion that ignores damping has been derived previously and its form is

$$\begin{aligned} \alpha &= C_1 \cos m_1 t + C_2 \cos m_2 t + \alpha_o \\ \beta &= C_1 \sin m_1 t + C_2 \sin m_2 t + \beta_o \end{aligned} \tag{3.1}$$

where α and β are the pitch and yaw components of the angle of attack, C_1 and C_2 are amplitude constants and m_1 and m_2 govern the rate at which the motion takes place. The description is a steady-state one and assumes that time is measured with reference to some arbitrary event; i.e., when the pitch angle is zero, for example. Trim angles are explicitly accounted for by the α_o and β_o terms.

Although the Equations (3.1) were derived for a spinning body, the description fits a wide variety of motion. Special cases are circular precession and planar oscillation, the first occurring with a spinning body in a force-free environment and the second due to retarding forces on a non-spinning body. The mathematical description also embraces other kinds of motion which cannot in truth occur because of physical restrictions.

To acquaint ourselves with typical variations in both the polarization and aspect angles under elliptical precession, we inserted hypothetical but realistic values for both the C's and the m's in (3.1). We then permitted time to run for 9 seconds and plotted the resulting aspect angle and polarization angle histories.

The roots m_1 and m_2 have the form

$$\begin{aligned} m_1 &= \omega (1 + A) \\ m_2 &= \omega (1 - A) \end{aligned} \tag{3.2}$$

where A is related,but not equal, to the acceleration of the body observed during flight, and ω is a radian frequency (not necessarily the vehicle spin). In the exo-atmosphere where retarding forces are small, A is very nearly unity; during the endo-atmospheric phase A is substantially bigger than this. In both the endo- and exo-atmosphere, a periodicity in the motion can usually be determined, although that of the latter is more difficult to estimate. Letting T_{ex} and T_{en} denote the respective periods of one cycle of motion, we can write that

$$2\omega T_{ex} = 2\pi,$$

$$\omega A T_{en} = 2\pi,$$

from which

$$\omega = \frac{\pi}{T_{ex}},$$

$$A = 2\frac{T_{ex}}{T_{en}}.$$

It follows that

$$m_1 = \pi\left(\frac{1}{T_{ex}} + \frac{2}{T_{en}}\right),$$

$$m_2 = \pi\left(\frac{1}{T_{ex}} - \frac{2}{T_{en}}\right).$$

Reasonable numbers for the periods are

$$T_{ex} = 10 \text{ seconds},$$

$$T_{en} = 2 \text{ seconds},$$

from which we calculate

$$m_1 = 1.1\pi = 3.456 \text{ rad/sec},$$

$$m_2 = -0.9\pi = -2.827 \text{ rad/sec}.$$

These are the motion rates that were used in the theoretical precession histories to be presented.

The size of the precession ellipse is dictated by the selection of C_1 and C_2 in (3.1). We originally planned four sizes for study, but one size was deleted in the interest of conserving space in the report. The table below shows the ellipse dimensions; note that the first is a circle.

C_1, degrees	C_2, degrees	Ellipse size, degrees x degrees
5	0	10 x 10
5	2	6 x 14
5	3	4 x 16

The ellipses, of course, represent body precession about the velocity vector; to get a selection of histories we chose mean aspect angles (μ) of 0, 5 and 10 degrees. This variety produces precession paths that, a) sweep around the line of sight, b) closely approach, but seldom encompass the line of sight, c) never approach or encompass the line of sight.

The results of the nine histories (three values of μ for each of three values of C_2) are displayed in Figs. 3-1 through 3-9. In the lower right hand corner of each, the initial orientation of the ellipse is shown as a dashed line, and the initial motion is indicated by a solid line tipped with an arrow. Because the ellipse axis advances while the elliptical path is traced out, the two do not coincide except for the special case of circular precession.

The aspect angle behavior is shown as a solid line and the polarization angle is dashed. All nine figures were plotted for a mean polarization angle of zero; if other mean polarizations are desired, the polarization angle traces need only be 'biased' by some constant angle equal to the mean polarization angle. The aspect angle histories, of course, would be unaffected.

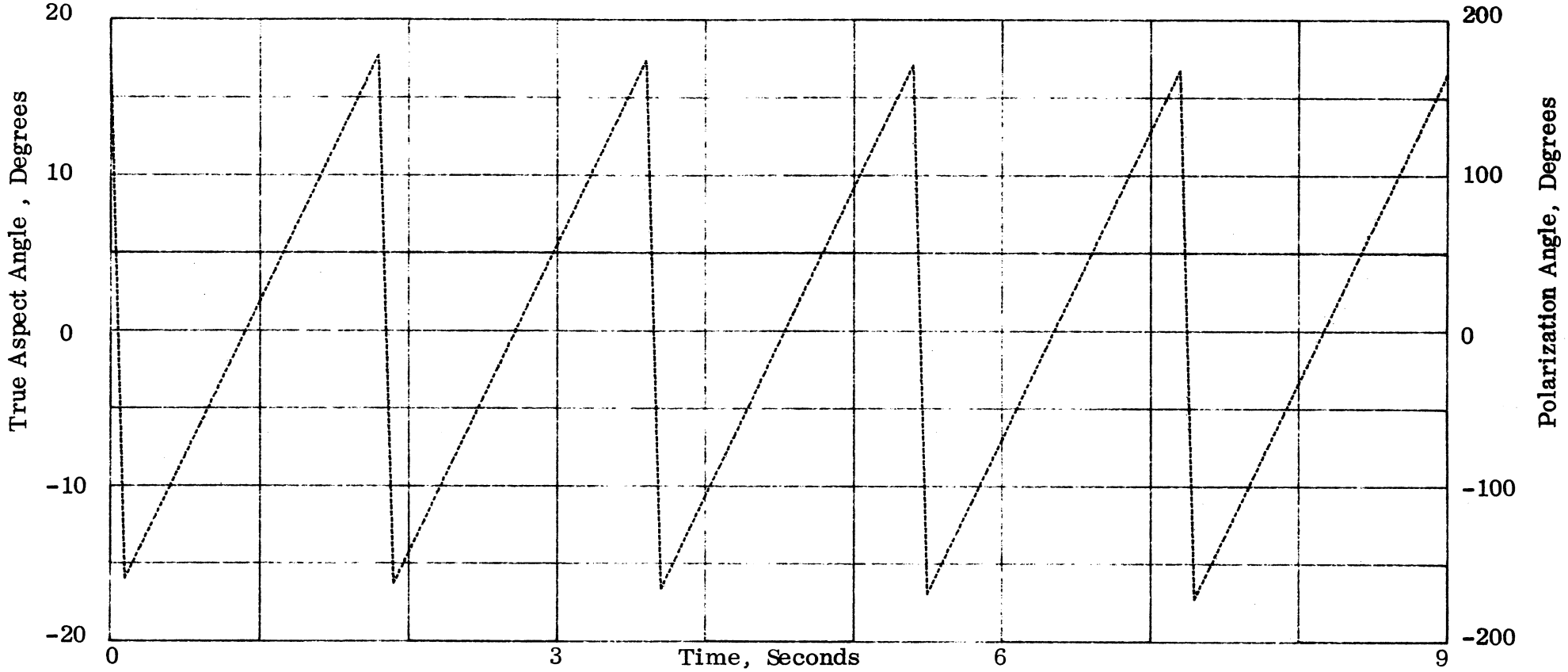

FIG. 3-1: Circular precession centered on the line of sight. Aspect angle is constant at 5^{o} in this case.

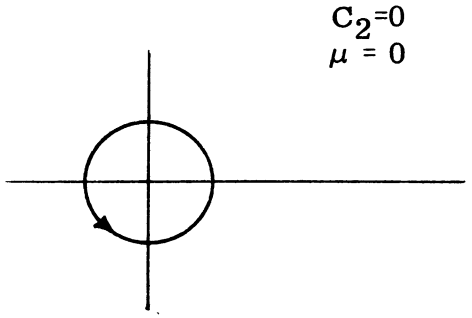

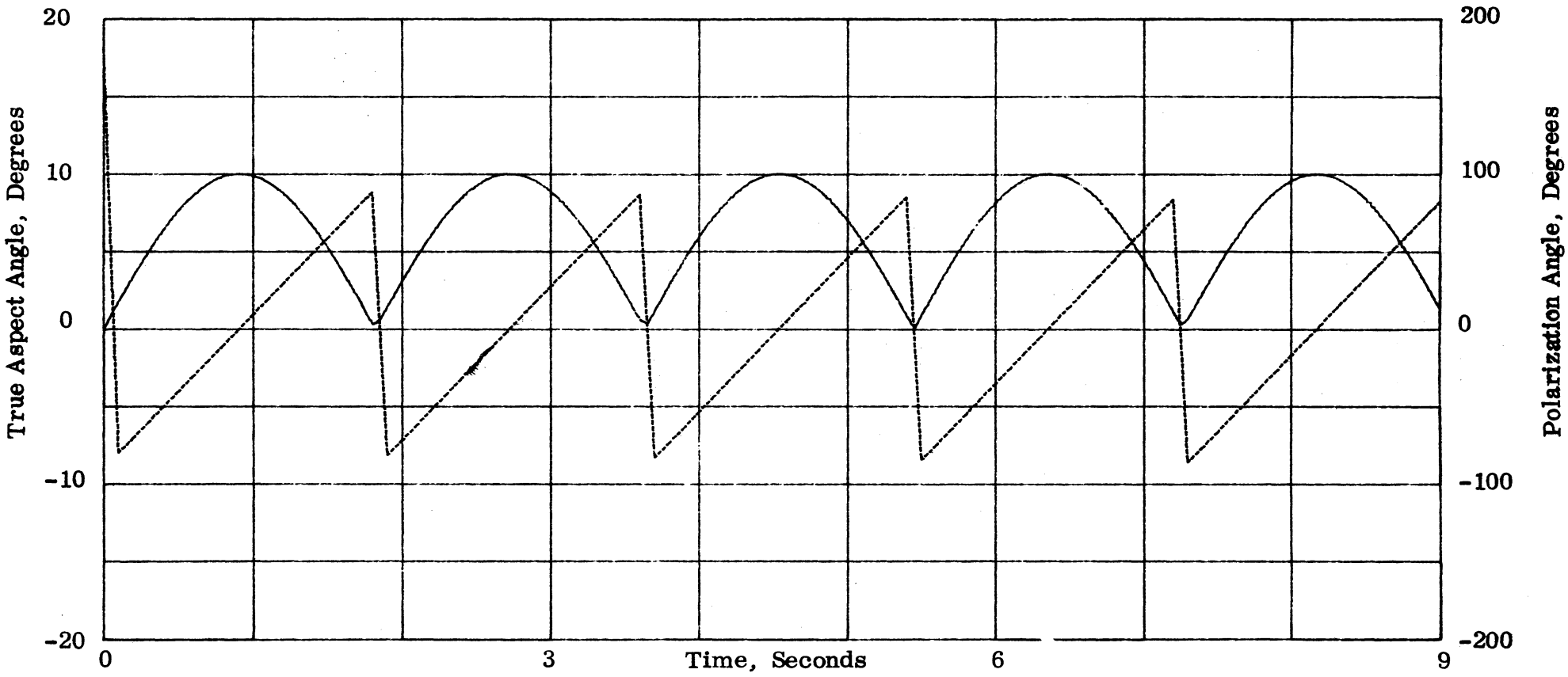

FIG. 3-2: Circular precession centered 5^{o} off the line of sight.

$C_2 = 0$
$\mu = 5$

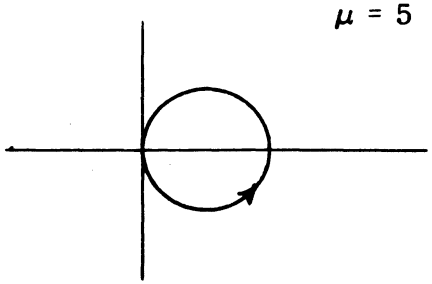

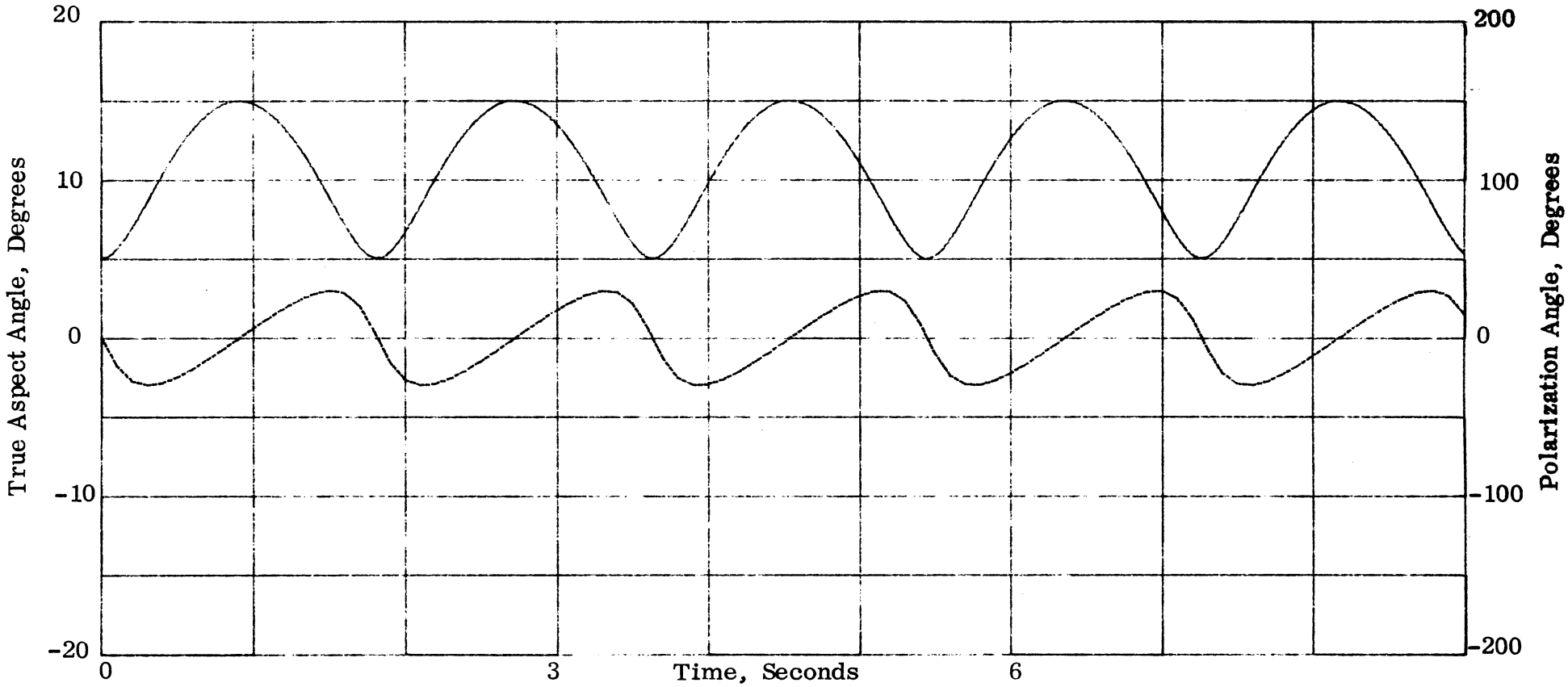

FIG. 3-3: Circular precession centered 10^{o} off the line of sight.

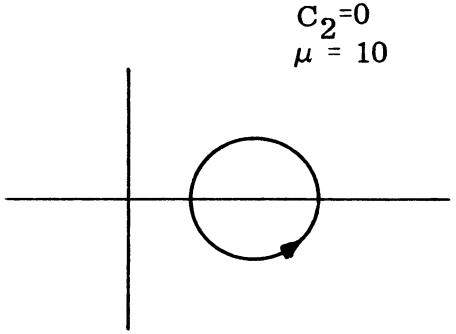

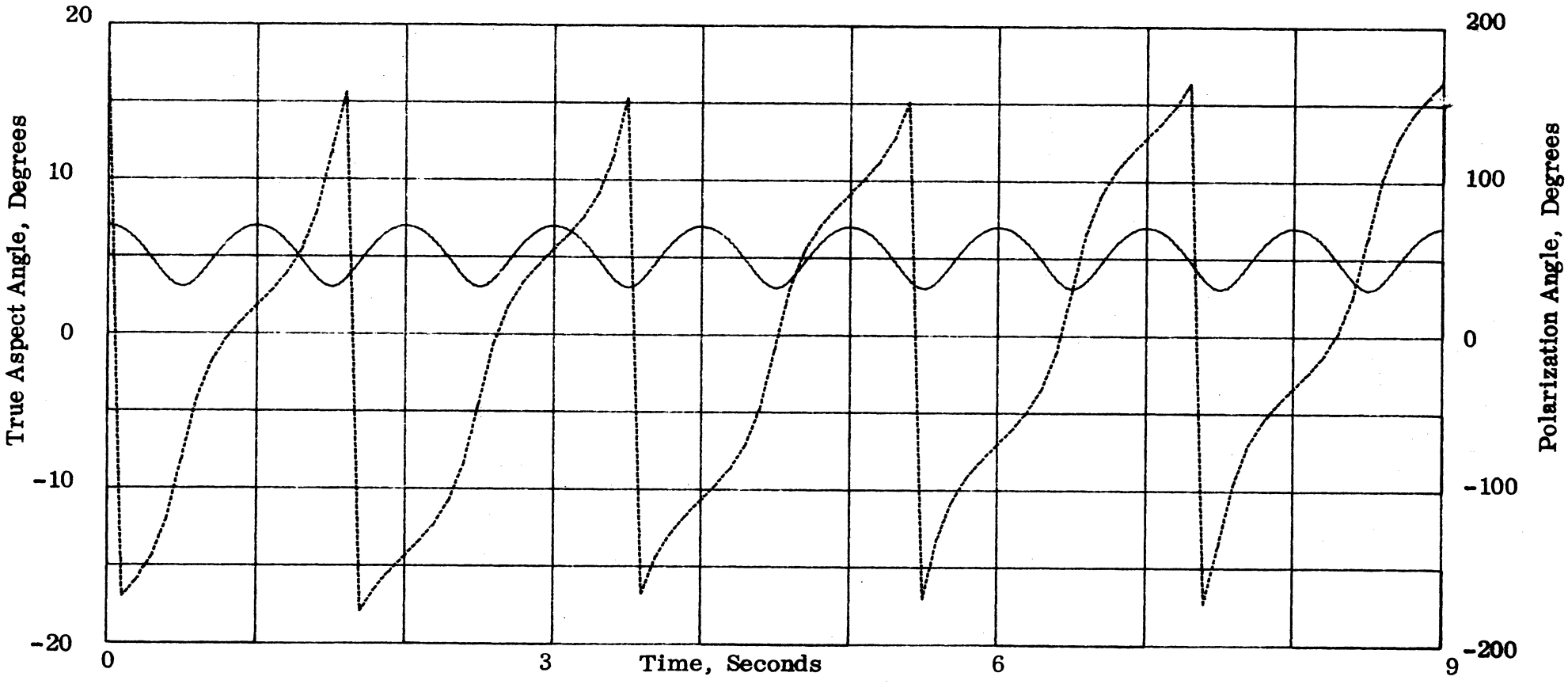

FIG. 3-4: Elliptical precession centered on the line of sight. Ellipse is 6° wide by 14° long.

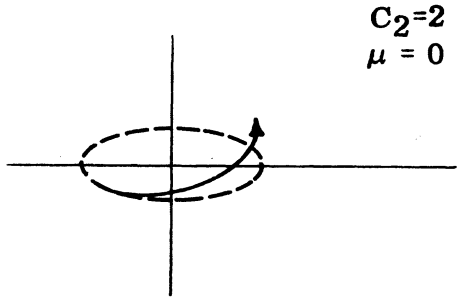

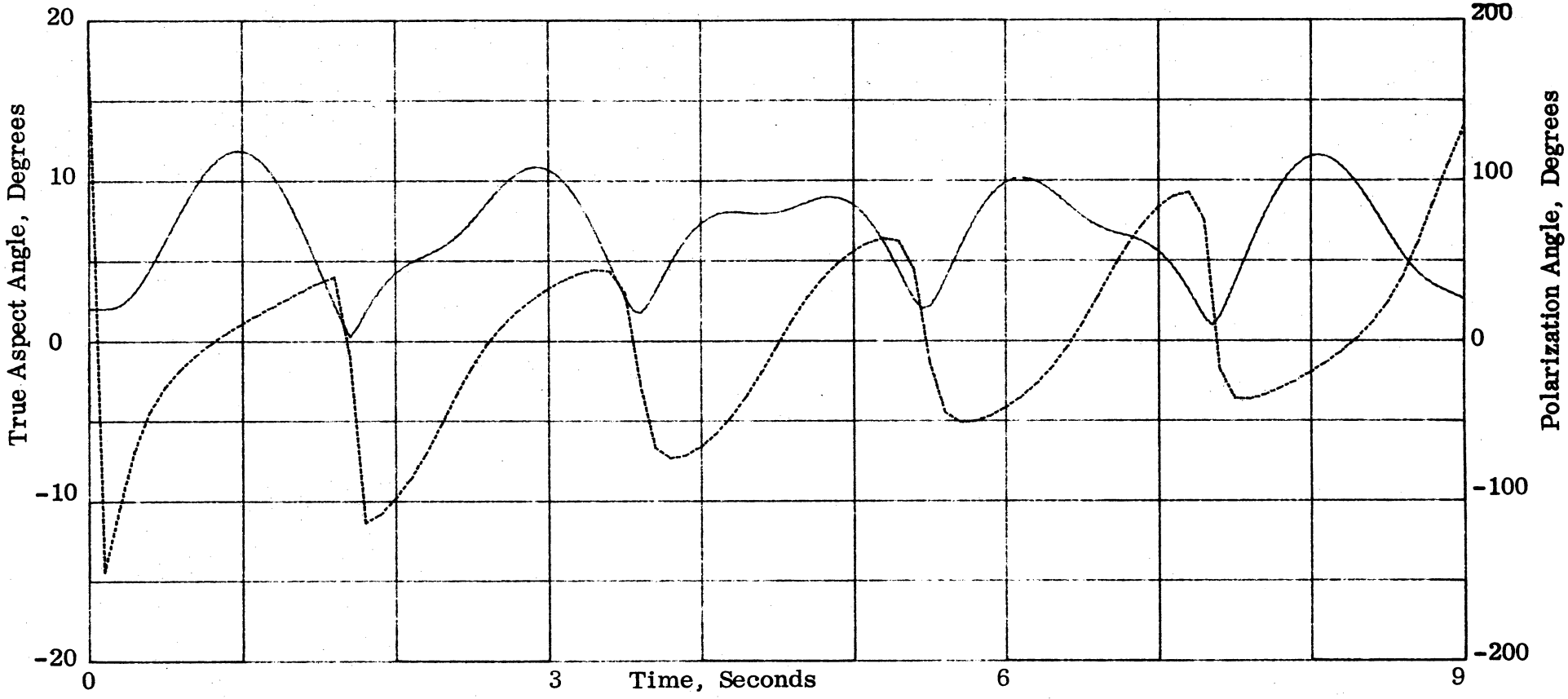

FIG. 3-5: Elliptical precession centered 5° off the line of sight. Ellipse is 6° wide by 14° long.

C_2=2
μ = 5

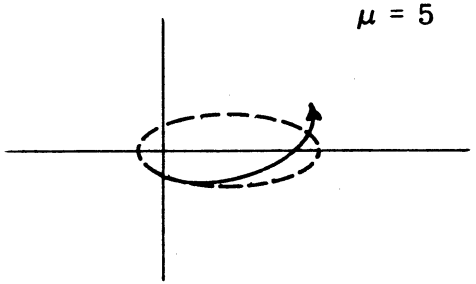

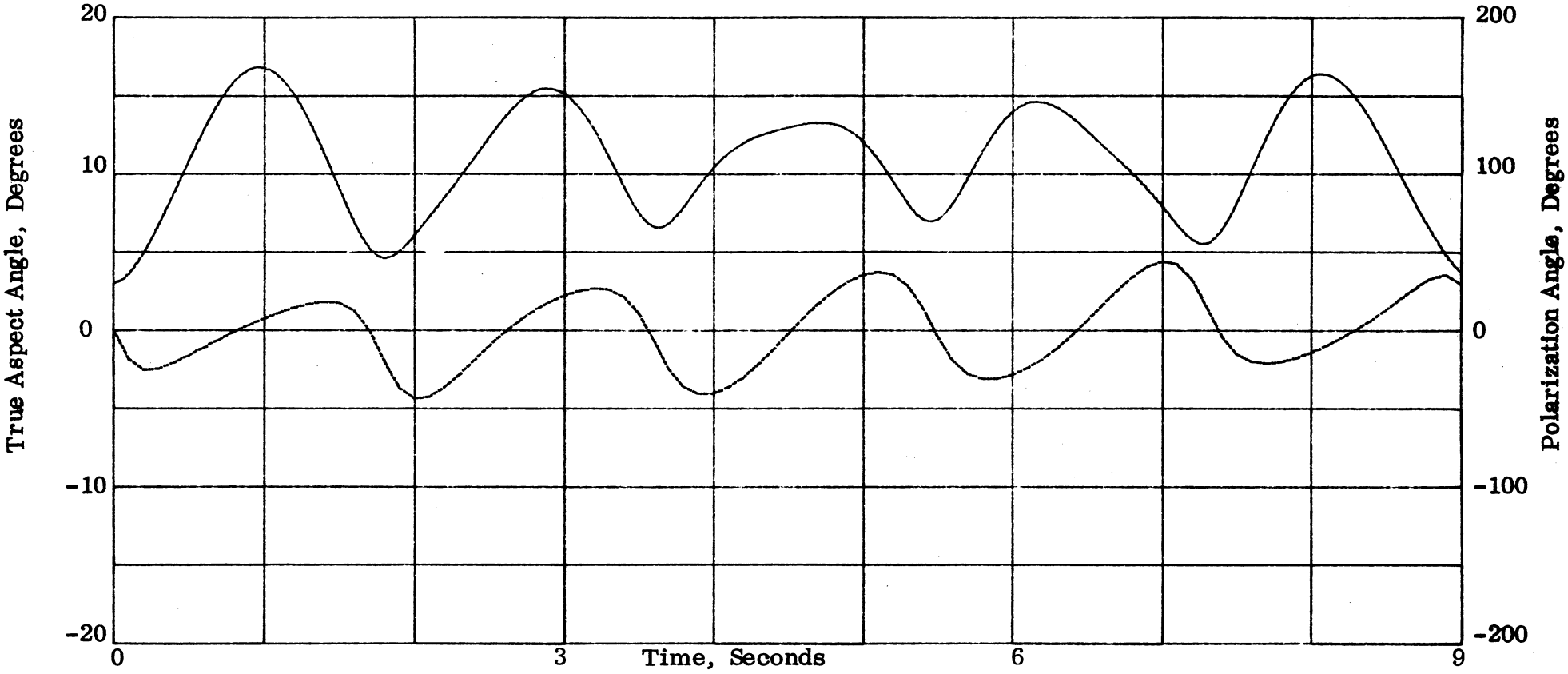

FIG. 3-6: Elliptical precession centered 10° off the line of sight. Ellipse is 6° wide by 14° long.

C_2=2
μ = 10

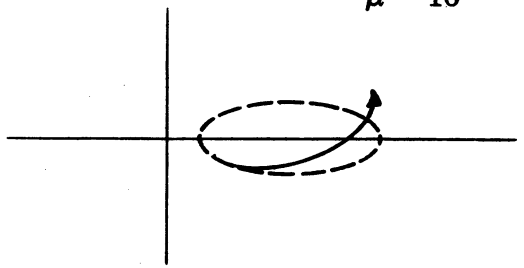

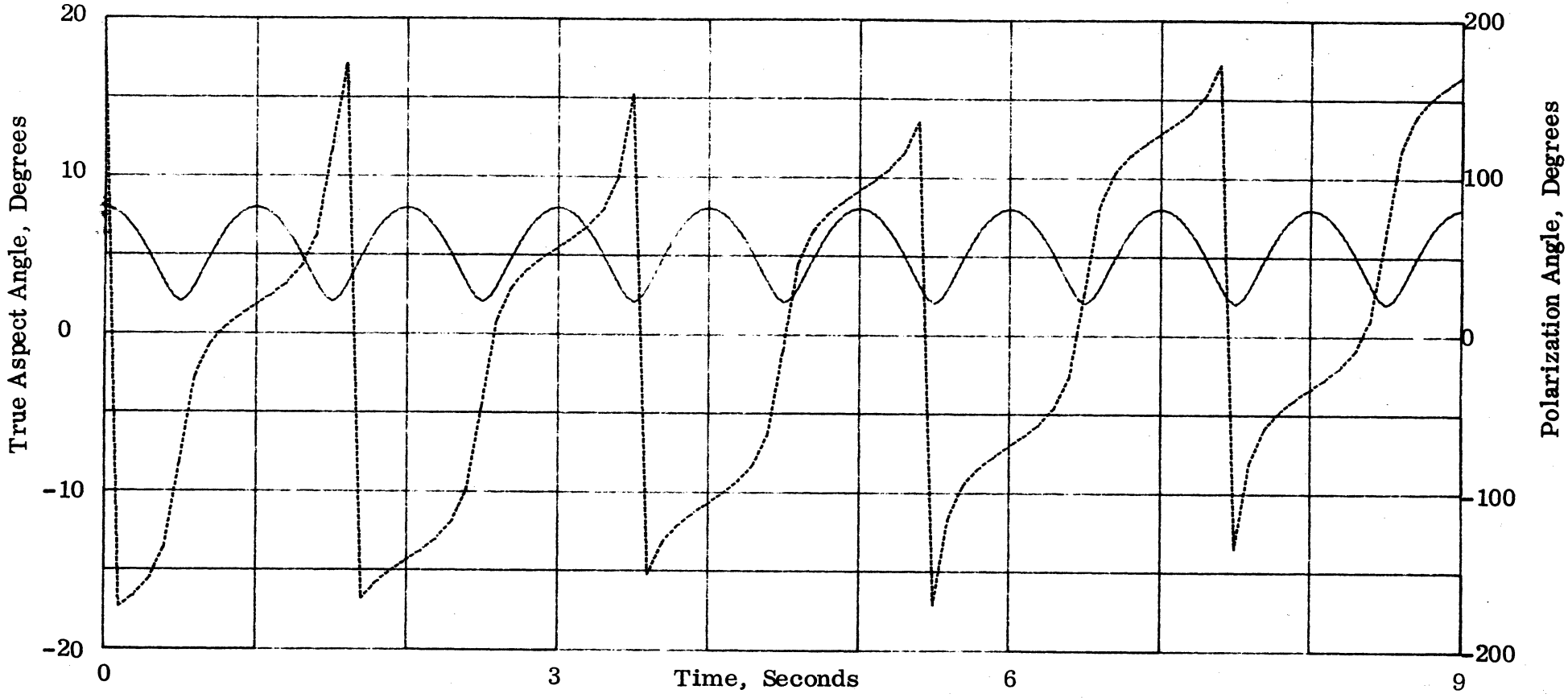

FIG. 3-7: Elliptical precession centered on the line of sight. Ellipse is 4^{o} wide by 16^{o} long.

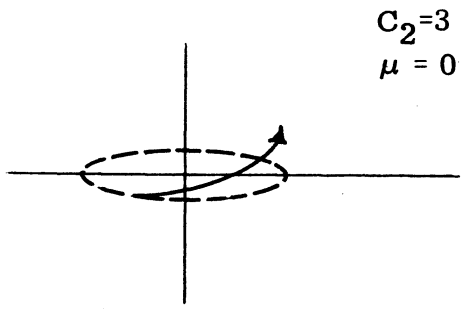

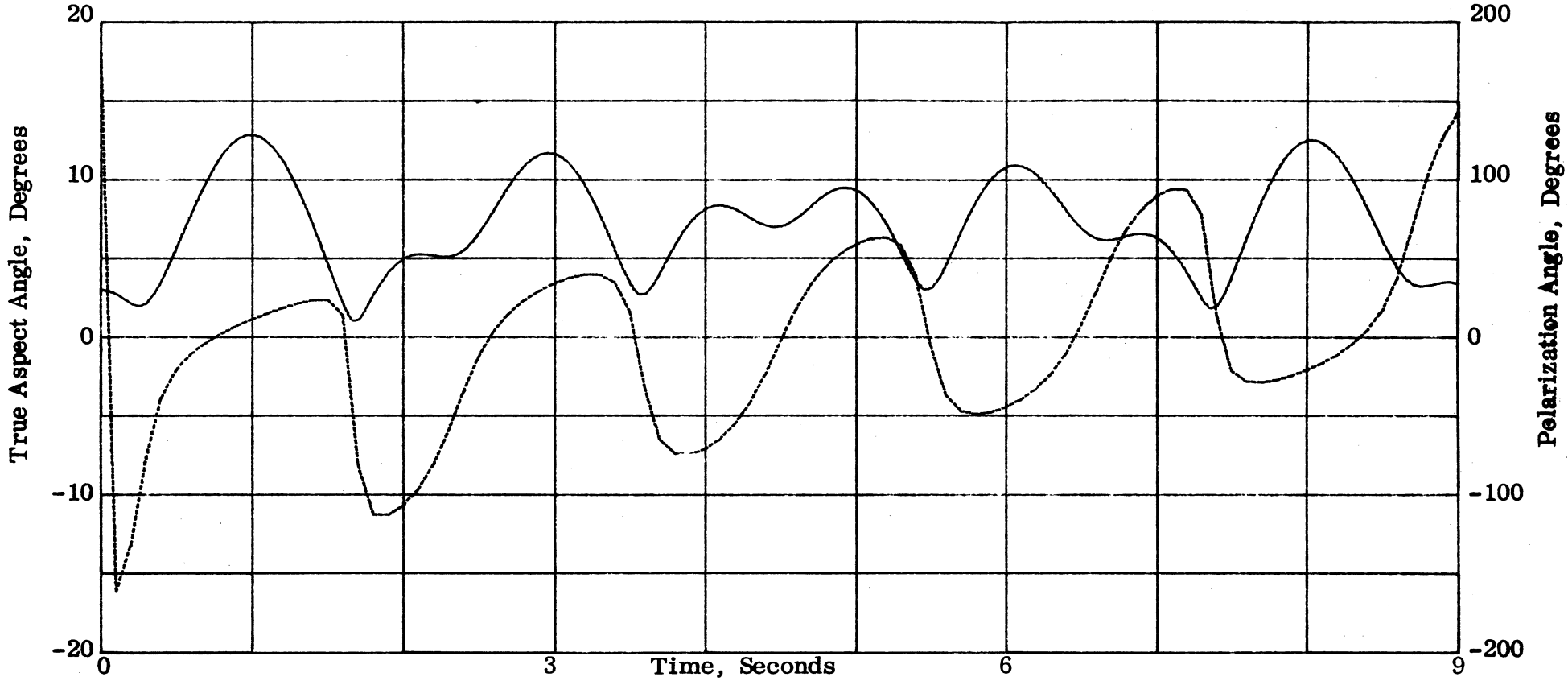

FIG. 3-8: Elliptical precession centered 5° off the line of sight. Ellipse is 4° wide by 16° long .

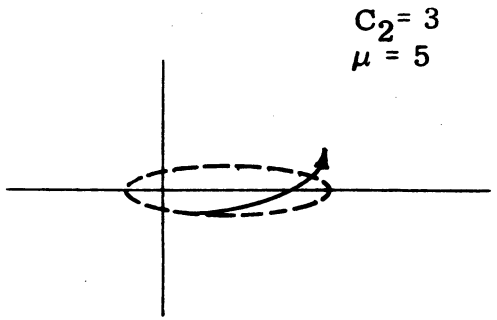

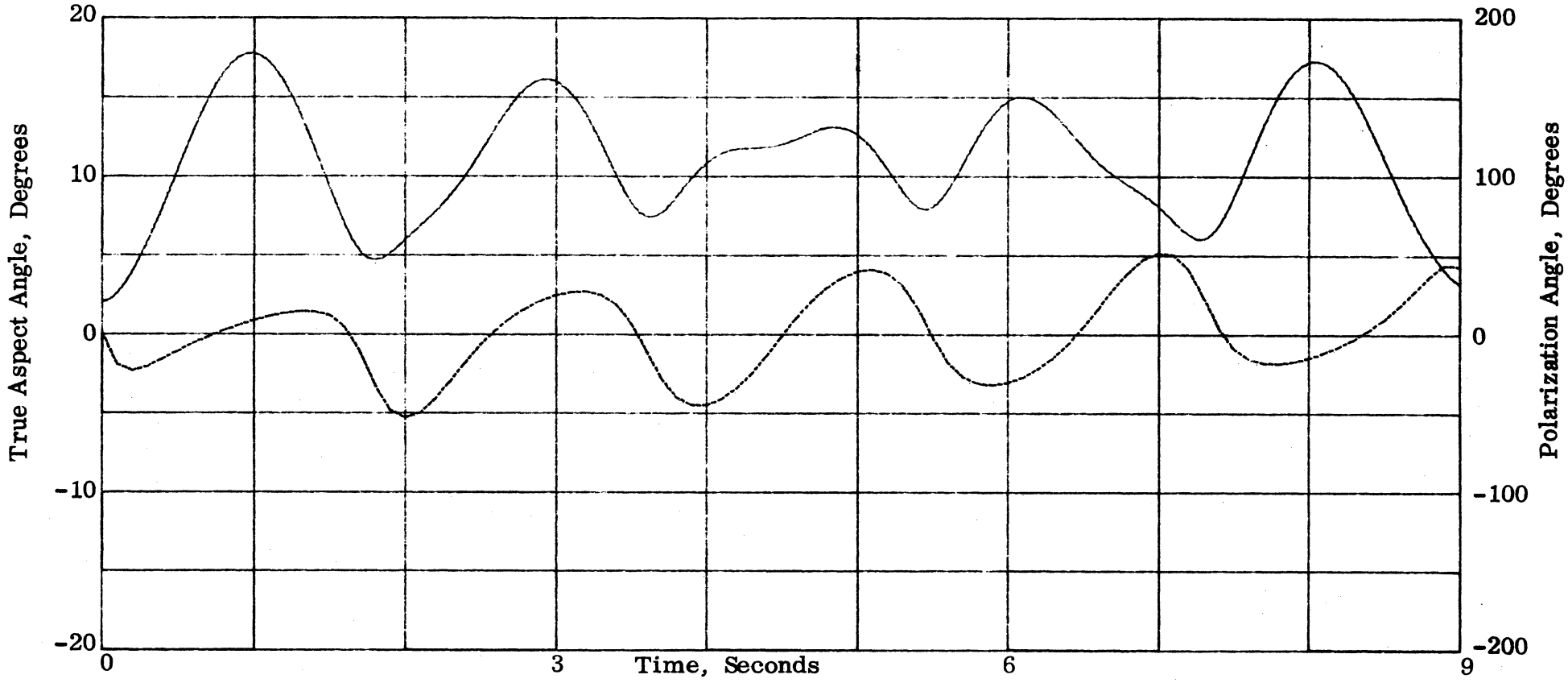

FIG. 3-9: Elliptical precession centered 10^{o} off the line of sight. Ellipse is 4^{o} wide by 16^{o} long.

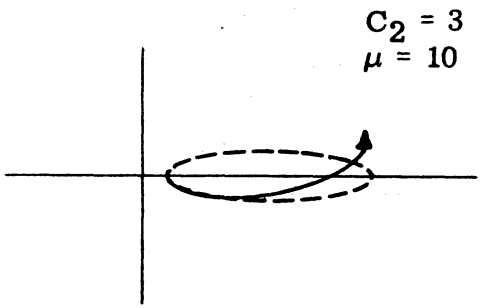

For circular precession centered on the line of sight (Fig. 3-1), the aspect angle is constant since the body is always seen at an angle equal to the precession cone half-angle. The polarization angle varies linearly with the angle around the precession cone and on the plot this produces a saw-tooth. In fact, as can be seen from Figs. 3-1, 3-4, and 3-7, a saw-tooth pattern prevails whenever the precession is centered on the line of sight, be it elliptical or circular precession.

Circular precession always produces a sinusoidal aspect angle history, in contrast to the saw-toothed polarization angle history, as shown in Figs. 3-1 through 3-3. The true polarization angle in this case always make equal excursions above and below the mean polarization angle (which is zero for all nine plots). Elliptical precession also produces a sinusoidal aspect angle histroy, but only when centered on the line of sight; the period is much shorter than that of circular precession not centered on the line of sight; compare Figs. 3-3 with Figs. 3-4 and 3-7.

Aside from the special cases just mentioned, elliptical precession is characterized by non-sinusoidal changes in both the true aspect angle and true polarization angles, even when the mean aspect and polarization angles are fixed. Unless we know beforehand that the precession is truly elliptical, for example, a casual inspection of Figs. 3-5, 3-6, 3-8 and 3-9 suggests that the mean angles are changing when in fact they are not. Thus the analysis of radar signature must be tempered with an awareness of these possibilities.

3.3 Getting Aspect Angle from Polarization Angle History

A thorough examination of the five-parameter method shows that it can produce principal plane returns and a polarization angle value based on a measurement of five parameters of a target's polarization scattering matrix, but that it does not give the aspect angle associated with these returns. There appears to be a way to accomplish this indirectly, through use of the polarization angle history; the time rate of change of the polarization angle is the

key. We will develop the method by assuming a body is undergoing circular precession, but the principle can be applied to other kinds of oscillatory motion.

The geometry of the precession is illustrated in Fig. 3-10; the precession circle has radius ρ and is centered on the velocity vector V, which in turn lies some angle μ from the line of sight, LOS. The target axis T follows the circle and the position of T at any time around the circle can be measured by the angle θ. The mean polarization ψ' is assumed fixed for simplicity and we seek to relate the true body polarization angle ψ to the position angle θ.

To be precise we must use spherical trigonometry, but since the complexity of doing so obscures the features we need to explain, we shall use plane trigonometry. If μ and ρ are small enough, say less than 20°, this is justifiable. By expressing the position of T in terms of its horizontal and vertical components, we can express the true polarization angle as

$$\psi = \arctan \left[\frac{\sin\psi' - r \sin (\theta + \psi')}{\cos \psi' - r \cos (\theta+\psi')} \right] , \tag{3.3}$$

where $r = \rho/\mu$ is the ratio of the precession circle radius to the mean aspect angle.

If both r and ψ' are held at fixed values, the time rate of change of the true polarization angle at each instant in time is

$$\dot{\psi} = \frac{r (r - \cos \theta) \dot{\theta}}{1 - 2 r \cos \theta + r^2} \tag{3.4}$$

where the dots indicate differentiation with respect to time. It will be convenient to work with angles θ that are either even or odd multiples of π, corresponding to minimum and maximum aspect angles respectively, whence we adopt the notation that

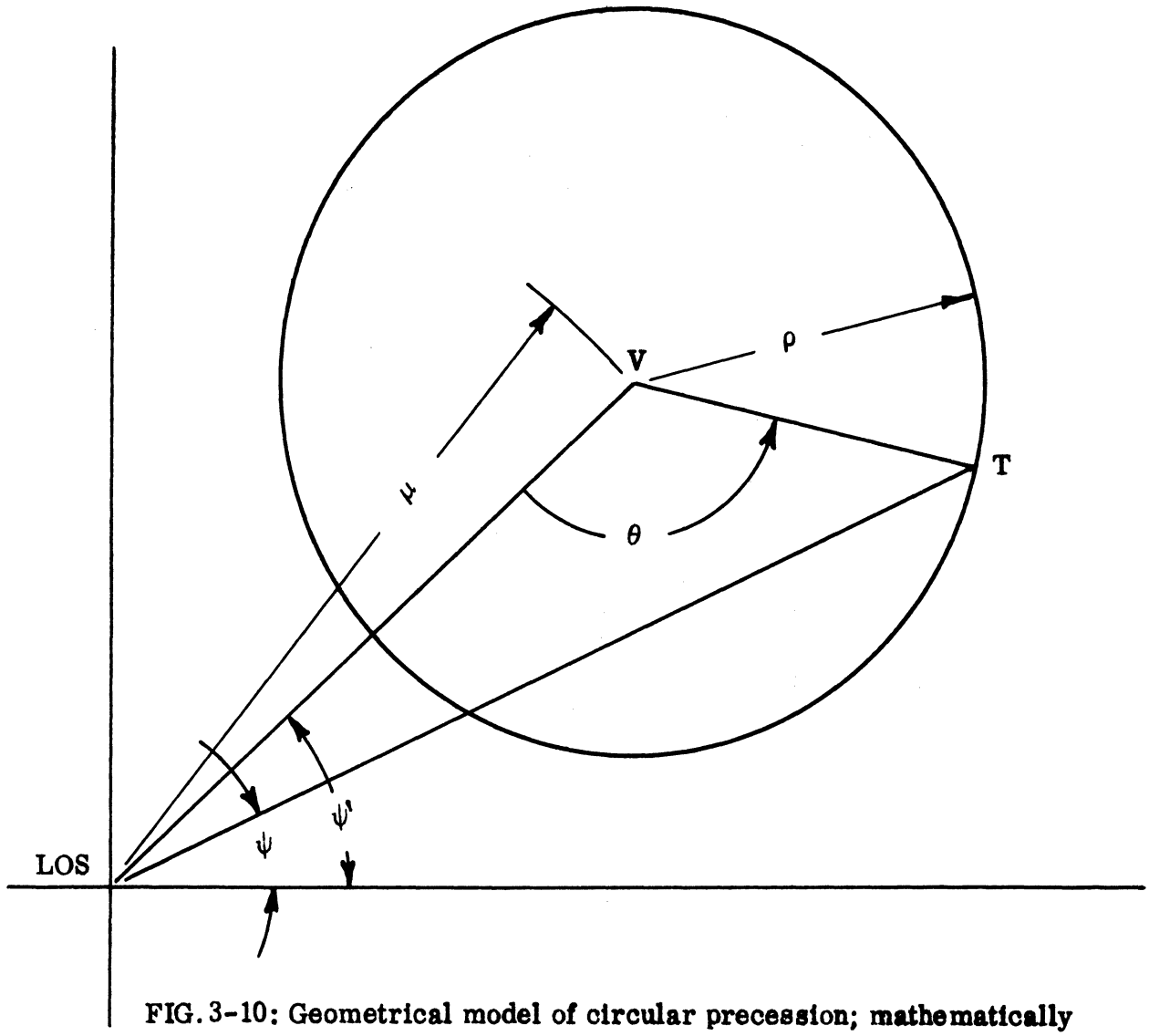

FIG. 3-10: Geometrical model of circular precession; mathematically we must relate true polarization angle ψ to the angle θ each instant in time.

$$\left.\frac{d\psi}{dt}\right|_{\theta=2n\pi} = \dot{\psi}_e ,$$

$$\left.\frac{d\psi}{dt}\right|_{\theta=(2n-1)\pi} = \dot{\psi}_o .$$

Thus, when $\theta = n\pi$ (3.4) can be solved for r with the subsequent result that

$$\rho = \frac{\mu\dot{\psi}_e}{\dot{\theta}-\dot{\psi}_e} , \tag{3.5}$$

$$\rho = \frac{\mu\dot{\psi}_o}{\dot{\psi}_o-\dot{\theta}} . \tag{3.6}$$

Note that we obtain two redundant bits of information for circular precession, one determined from $\dot{\psi}_e$ and the other from $\dot{\psi}_o$. The mean aspect angle μ is, of course, available from metric data, so that, if the five-parameter method is available, it promises to give us aspect angle information by combining polarization angle data (as determined from signature information) with metric data.

It is of interest to apply the results (3.5) and (3.6) to the polarization angle trace of Fig. 3-3. We took a copy of the figure, made a work sheet of it, the result of which is Fig. 3-11. Note that we firstly establish the periodicity, and thence $\dot{\theta}$, of the polarization angle history; this comes out as 1.82 seconds, or 199 deg/sec. The maximum positive slope of the trace is 66 deg/sec and the maximum negative slope is -188 deg/sec. These values were obtained by scaling the graph with dividers and straight-edge, as might be done with real-world data.

Since ψ changes faster near $\theta = (2n-1)\pi$ than it does near $\theta = 2n\pi$, the maximum rate of change is associated with the odd value of $\dot{\psi}$. We deduce that

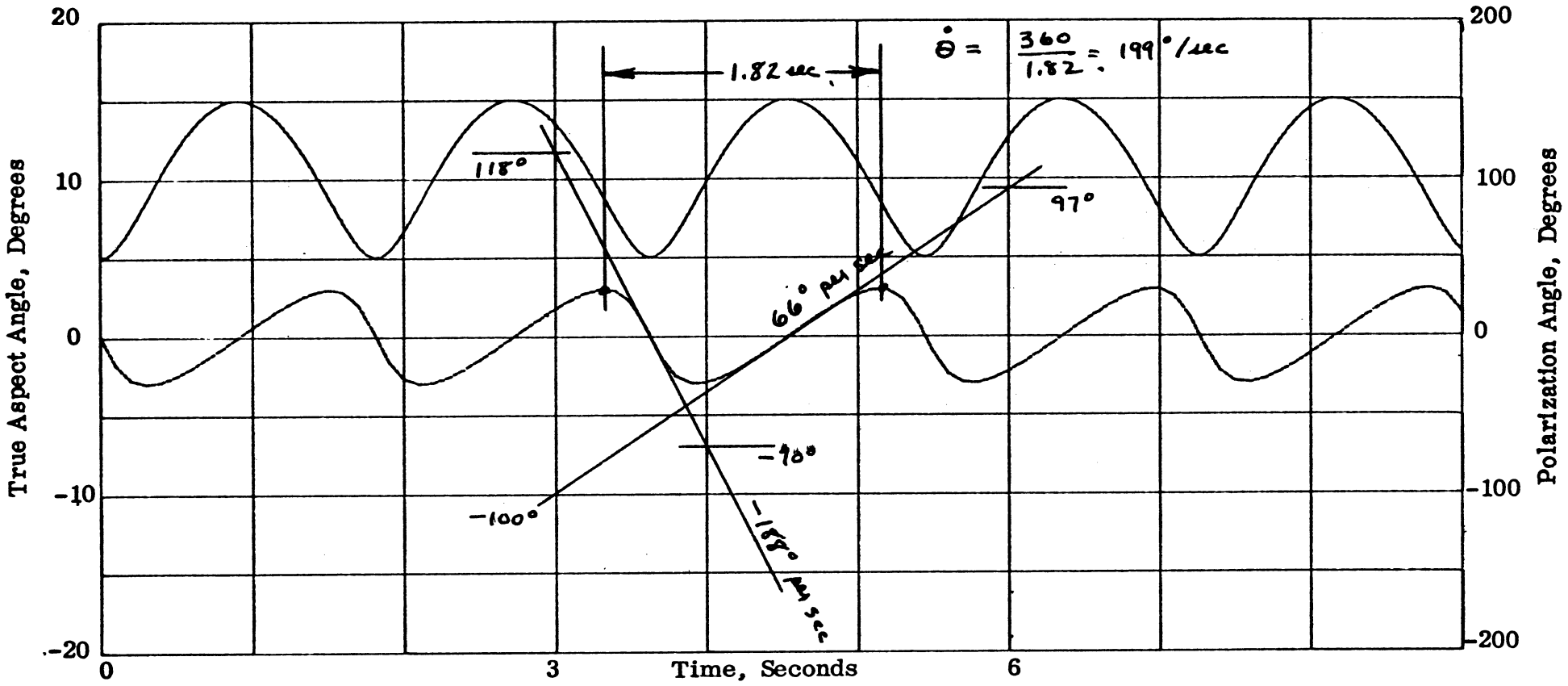

FIG. 3-11: We made a worksheet of Figure 3-3 and used it to test the aspect-angle-from-polarization-angle method. The upper trace (true aspect angle) was ignored for this test.

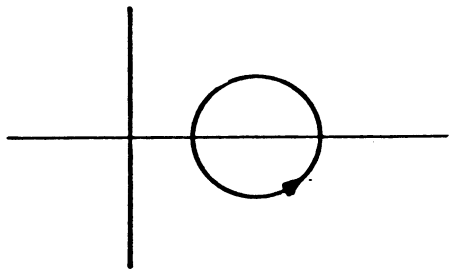

$\psi_e = 66$ deg/sec,

$\psi_o = -188$ deg/sec.

For this test we know that $\mu = 10^o$; testing each value in the appropriate expression (3.4) or (3.5), we find that

$$\rho = \frac{(10)\ (66)}{199 - 66} = \frac{660}{133} = 4.96 \text{ degrees},$$

$$= \frac{(10)\ (-188)}{-188 - 199} = \frac{1880}{387} = 4.86 \text{ degrees}\ .$$

The true value of ρ was 5 degrees and the errors contributed by the use of plane trigonometry and graphic scaling of the data amount to less than 3 percent. We conclude that the technique is straightforward and effective under the conditions of the test, and offers a powerful incentive to equip the Advanced Range Instrumentation Ships with instruments required by the five-parameter method.

Note that the method produces two redundant values for the case of circular precession because it requires only one parameter to describe a circle. An ellipse on the other hand, is defined by no fewer than three quantities, two of which specify its size and one of which specifies its orientation. This means that a third feature of the polarization angle history, in addition to the two we have already suggested, must be defined in order to determine the elements of elliptical precession. Neither time nor funding permitted us to embark upon a more general study of the applications of polarization angle data, but such an effort is clearly desirable, if not necessary, if such data are to be collected.

IV

THE H0037, H0039 AND H0041 TRIAD

(U) This Chapter contains a sequence of three related Test Support Missions, showing that differences as well as similarities exist, and is printed as Volume 2 to this Final Report. That Volume is Secret and copies may be obtained from the Air Force Eastern Test Range, Attn: ETEQO, Patrick Air Force Base, Florida 32925 , upon approval from the Foreign Technology Division, TDD, Wright-Patterson Air Force Base, Ohio 45433.

This Chapter is Unclassified

V

SCATTERING FROM DISKS AND CONES

5.1 Introduction

The success of any target identification or sizing scheme based on radar ultimately rests on our ability to recognize the radar signature as being that associated with a specific geometry. Thus, for example, the five parameter sizing scheme has as its output the principal plane returns as functions of time, thereby removing from the original data the considerable complication represented by the changing polarization angle. But even if one is successful in converting these reduced patterns to functions of target aspect rather than time, the scheme will be of practical utility only if one can interpret or recognize these patterns to provide information about the geometry and size of the target. To carry out this last step generally requires a detailed knowledge of the direct scattering from selected simple but relevant geometries, together with an appreciation of how slight perturbations in the geometry will affect the scattering.

If the range of aspects spanned by the data is such as to include one or more specular returns, the resulting peaks are usually dominant, and sizing schemes based on analysis of such specular peaks and their associated side-lobes are already in existence. We note that over these aspect ranges any cross polarized return is generally negligible by comparison. However, in the ARIS data, the target is seldom viewed at an aspect corresponding to a specular return. This is particularly true in the exo-atmospheric situation where the aspects are generally in a vicinity of nose-on, and the focus of our endeavour has been the development of viable identification and/or sizing schemes appropriate to this aspect range.

For cone-like bodies with a nose-radius which is not comparable to the length, the near nose-on return is smaller than the specular return from the slant side. Precisely at nose-on there is, of course, no cross-polarized return if the body is rotationally symmetric, but at some aspect a few degrees away from axial, the cross polarized return generally displays a strong peak which may be almost as intense as the on-axis return. The exploitation of this peak is the basis of the cross-polarized sizing scheme referred to in Chapter 3.

Whereas the aspect range around broadside to the vehicle is one where cross polarized effects are relatively small, to ignore these effects in the near nose-on range is to deprive oneself of a great deal of information about the target. Until the advent of the work carried out under the present contract, relatively little was known about the cross-polarized return. It is true that the occurrence of a near nose-on lobe for a right circular cone was indicated by an approximate analysis of Ross (1967), but confirmation was obtained only by a systematic series of experiments carried out under this contract, which experiments showed that the intensity of this peak increases with the "edginess" of the target.

Since a detailed description of the direct and cross polarized returns requires more than the sort of physical optics or "first order" analysis available, a systematic program of theoretical and experimental investigations was undertaken aimed at the understanding of the near nose-on behavior of cone-like objects. The first body studied theoretically was the disk. This is the limiting case of a right circular cone as the interior cone angle approaches 180°, and is, perhaps, the most "edgy" shape that can be imagined. However, the real reasons for starting with the disk were its geometrical simplicity (the infinitesimally thin disk is defined by only one parameter, its radius, a),

and the fact that the scattering problem is capable of exact analysis. The exact solution takes the form of a doubly infinite series of oblate spheroidal wave functions and is convenient for computation only if ka is not too large (say $ka \lesssim 6$). The resulting values for the back scattered field are in excellent agreement with experimental data.

It is obvious that an exact solution, or a series of accurate experimental measurements, is of considerable value in its own right, but each is of still more value as a means of checking (or suggesting) an asymptotic or other formula which can pinpoint those features of the target responsible for the dominant contributions to the scattering. Not only are asymptotic formulae more appropriate to the frequency ranges of direct interest to us, but in general they are also capable of application to more complex shapes. Even if it were possible to compute an exact solution for every target shape of interest, it would be economically prohibitive to do so for all aspects and all parameter combinations. We have therefore given considerable attention to the development of adequate asymptotic expressions to represent the back scattering behavior of a disk. By pushing the geometrical theory of diffraction to a higher order than has previously been done, certain new ray paths have been discovered describing the cross-disk interactions. The resulting expressions for both the direct and cross polarized back scattered fields are in very good agreement with experiment providing the effect of finite disk thickness is taken into account.

Although the disk is not itself a shape of interest in the ARIS program, we undertook our detailed study confident in our ability to extend any asymptotic treatment to the more practical case of a right circular cone. This confidence has been justified, and in Section 5.3 we present a second order asymptotic formula for the back scattered field at angles near to nose-on incidence. In particular, the polarization effects are displayed, and for horizontal polarization

the results are well supported by experiment. We have also provided a continuation of the expression which is adequate for the prediction of the back-scattered field out to the angle of the specular flash from the slant side of the cone. For vertical polarization, time has not permitted us to go beyond a first order expression for the field, though only a few more days of effort would have enabled us to derive the second order terms in this case also. Unfortunately, this must now await a continuation of the study, as must a consideration of cones with more general terminations.

All of the above analyses have been carried on in parallel with a measurement program. In many cases the key to the development of a theory has come from a study of experimental data, and at all stages we have sought to confirm our theoretical predictions in the laboratory. The importance of such measurements cannot be overemphasized, not only as an aid to theory, but also for revealing trends that could be used for target sizing (as, for example, in the cross polarized sizing scheme) and for verifying interpretations of ARIS data by direct laboratory simulation using the postulated target and its motion. A survey of some aspects of the measurement program is given in Section 5.4.

5.2 Disks

Consider an infinitesimally thin, perfectly conducting disk of radius a lying in the xy plane with the center at the origin of the Cartesian coordinate system (x, y, z). The disk is illuminated by a plane electromagnetic wave incident in the yz plane in a direction making an angle Φ with the negative z axis. It is convenient to treat separately the two cases of vertical (V) polarization in which

$$\underline{E}^i = \hat{x}\, e^{-ik(y \sin \Phi + z \cos \Phi)} , \tag{5.1}$$

and horizontal (H) polarization in which

$$\underline{E}^i = (\hat{y} \cos \phi - \hat{z} \sin \phi)\, e^{-ik(y \sin \Phi + z \cos \Phi)} , \tag{5.2}$$

the time factor $e^{-i\omega t}$ being omitted. In the former case, the backscattered electric field can be written as

$$\underline{E}^{s} = \hat{x} \frac{e^{ikr}}{kr} S_V \quad , \tag{5.3}$$

whereas in the latter

$$\underline{E}^{s} = (\hat{y} \cos\phi - \hat{z} \sin\phi) \frac{e^{ikr}}{kr} S_H \quad , \tag{5.4}$$

where r is the distance from the center of the disk. In terms of the far field amplitude S, the backscattering cross section is

$$\sigma_{V,H} = \frac{\lambda^2}{\pi} \left| S_{V,H} \right|^2 \quad . \tag{5.5}$$

We remark that if the incident electric vector is incident at an angle ψ to the (y, z) plane, the electric vector in the back scattered field will have components parallel and perpendicular to the incident vector. The latter constitutes the cross polarized component, and if $\psi = 45^{o}$,

$$S_{cr} = \pm \frac{1}{2} \left| S_V - S_H \right| \quad , \tag{5.6}$$

implying

$$\frac{\sigma_{cr}}{\lambda^2} = \frac{1}{4\pi} \left| S_V - S_H \right|^2 \quad , \tag{5.7}$$

As noted earlier, the problem that we have just formulated is capable of exact solution., Following Flammer (1953), the incident and scattered fields are expanded in terms of eigenfunctions in oblate spheroidal coordinates, leading to expressions for $S_{V,H}$ as doubly infinite series of oblate spheroidal functions with known coefficients (see Knott et al, 1969 for details). The problem is thereby

reduced to a computational one, and using the tables of spheroidal function coefficients given by Stratton et al (1956), reinforced with such additional computations as were required, values were obtained for $S_{V,H}$ at 2^{o} increments in Φ for a sequence of ka. A complete discussion of the theory and computation can be found in Mattson (1970a, see also 1970b) where it is pointed out that because of limitations in the available tabulations the computer program is effective only for $ka \lesssim 7$. Typical of the results obtained from this study are those for ka = 4 shown in Figs. 5-1 through 5-3. The computed data are in excellent agreement with measured values for a disk 1.127 inches in radius and 0.005 inch thick taken at a frequency of 10.0 GHz.

For sufficiently large ka, the far field coefficients S_V and S_H can be expanded asymptotically in series of inverse (fractional) powers of ka, and we now turn to a consideration of the first two terms of these series.

Using the geometrical theory of diffraction, Keller has shown that for axial incidence ($\Phi = 0$):

$$S_{V,H} \sim \frac{1}{2} i(ka)^2 - \frac{1}{2}\sqrt{\frac{ka}{\pi}}\, e^{i(2ka - \frac{\pi}{4})} + O(1) , \qquad (5.8)$$

where the first term is attributable to direct scattering from the rim, and in the direction of the axial caustic is equivalent to the physical optics contribution, and the second term is attributable to interactions between all diametrically opposed elements of the rim. It is convenient to speak of these as first and second order terms respectively.

When the incidence is well away from normal ($2ka \sin \Phi >> 1$), the application of the geometric theory has hitherto been limited (Keller, 1962; Bechtel, 1965) to the determination of the first order terms corresponding to direct edge scattering from the two diametrically opposed 'flash' points specified by the theory, giving

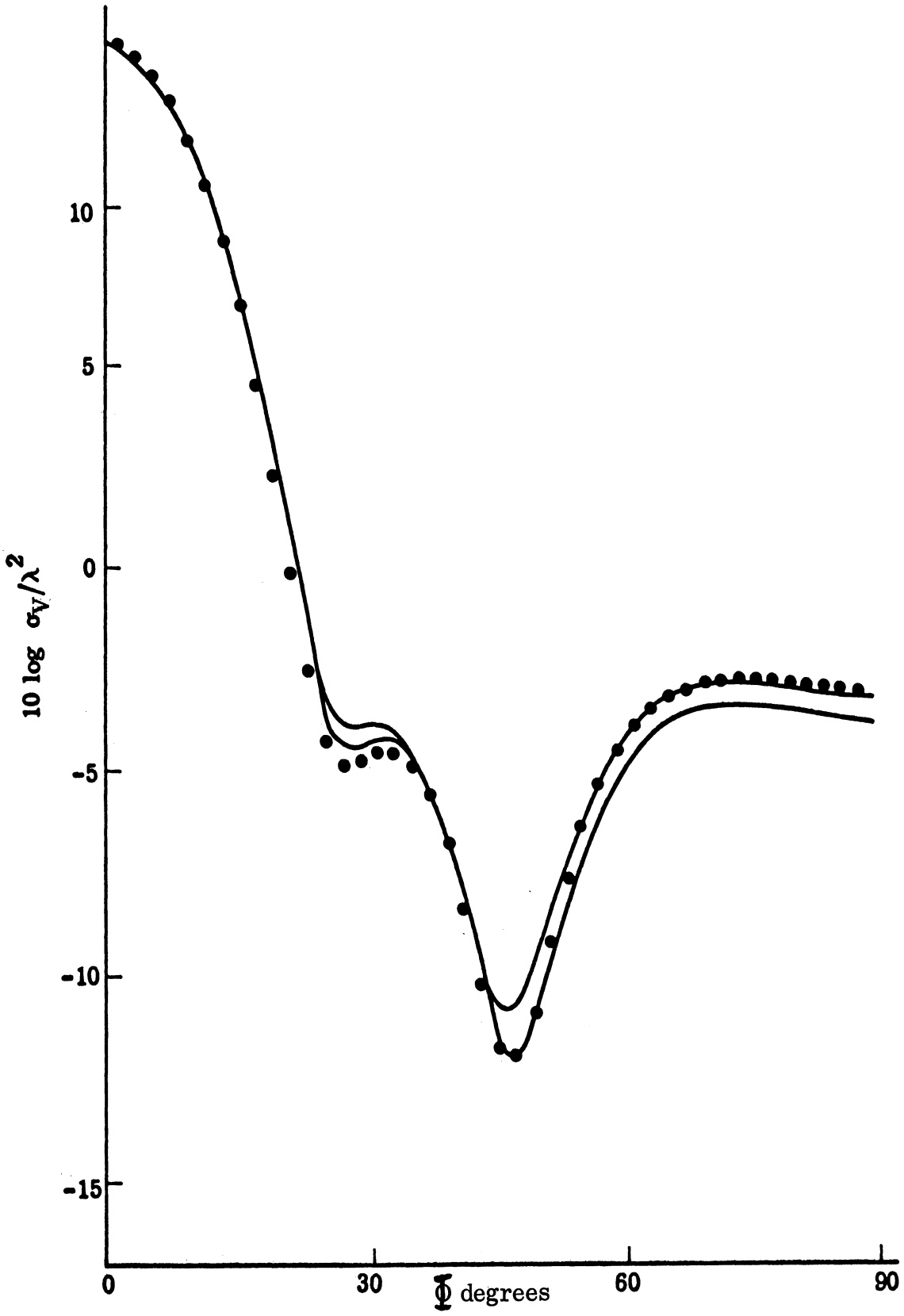

FIG. 5-1: Comparison with exact theory (●●●) with experiment for V polarization with ka = 4.

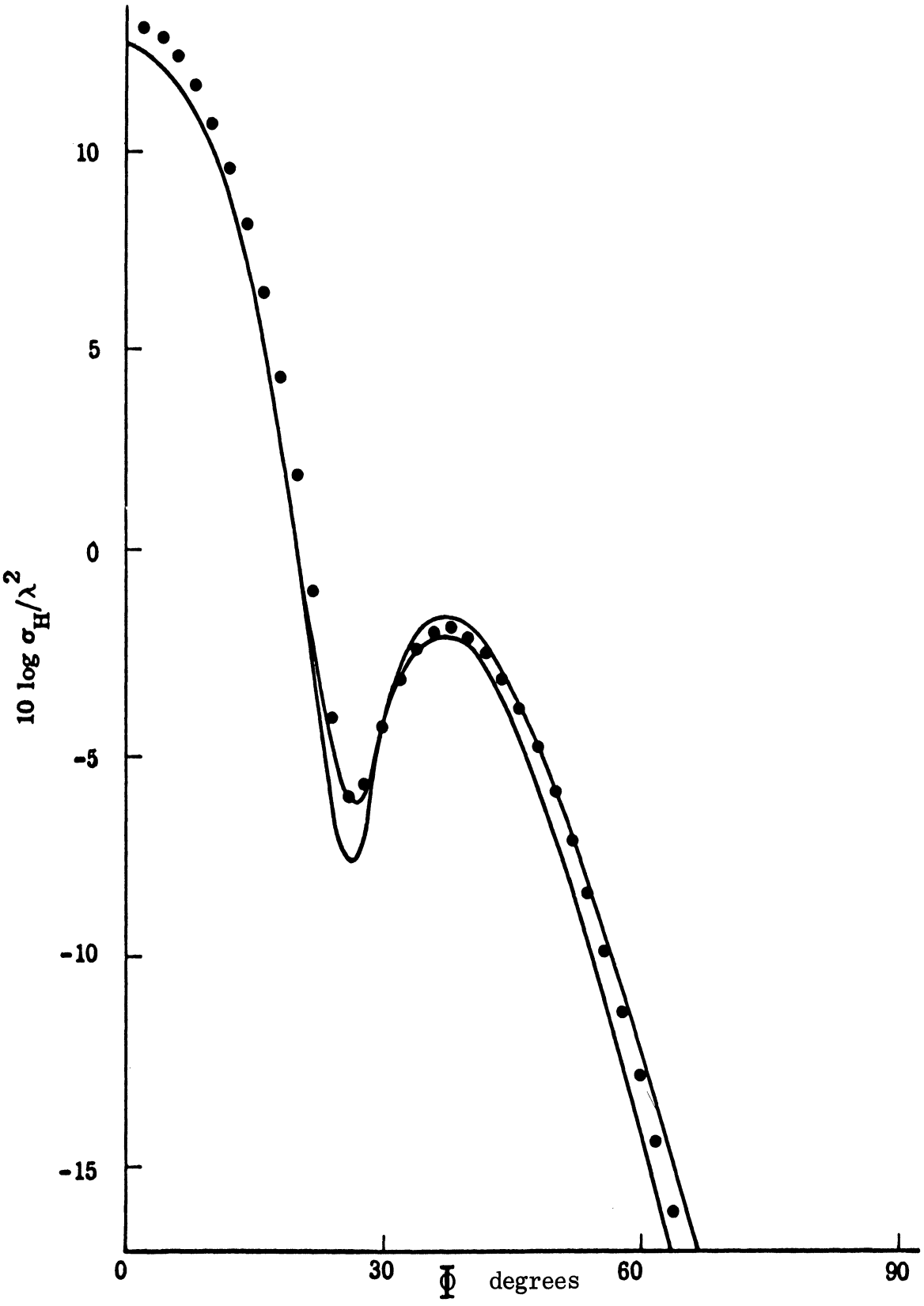

FIG. 5-2: Comparison with exact theory (• • •) with experiment for H polarization with ka = 4.

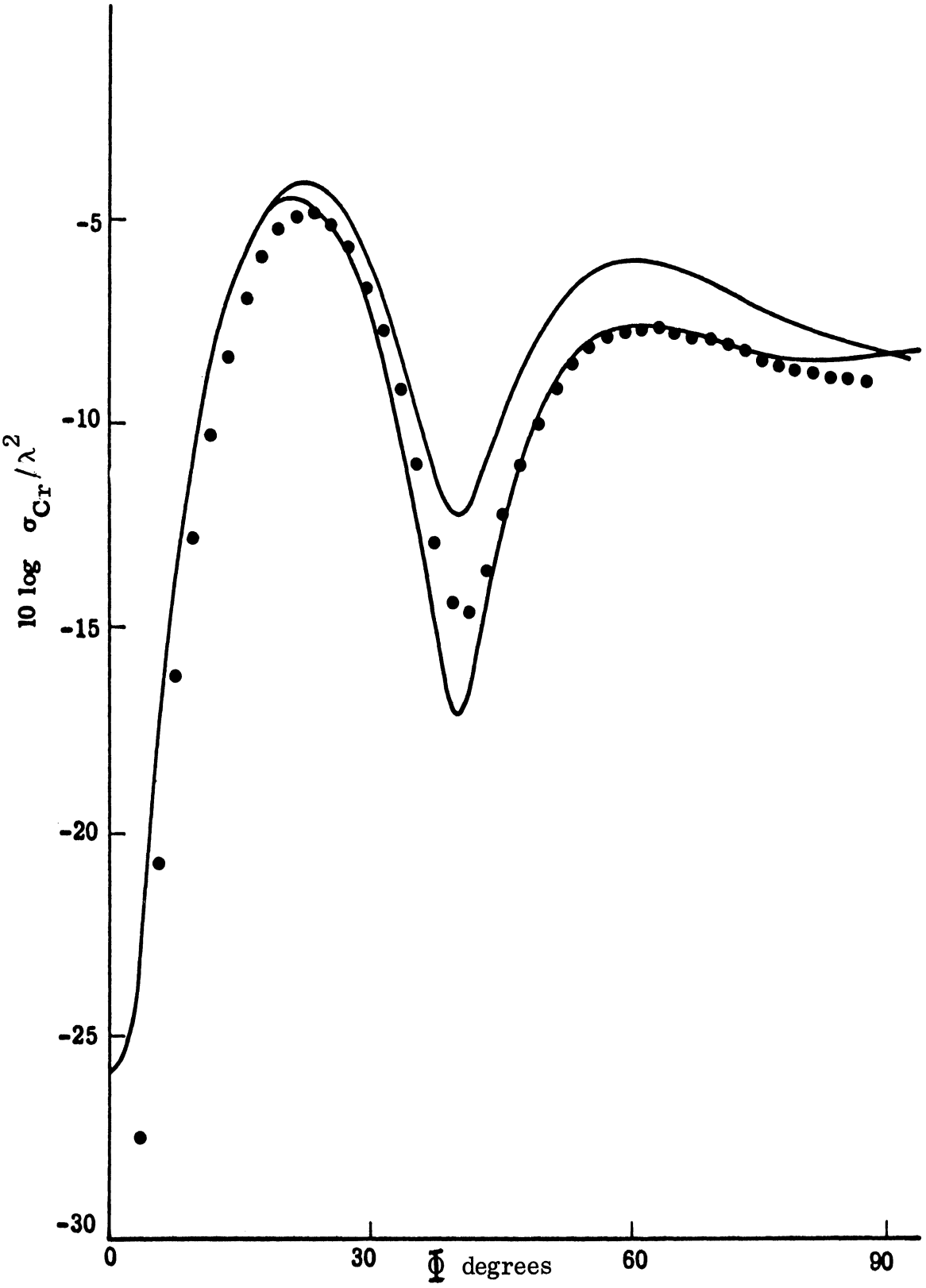

FIG. 5-3: Comparison with exact theory (•••) with experiment for cross polarization with ka = 4.

$$S_{V,H} \sim \frac{1}{4}\sqrt{\frac{ka}{\pi \sin\Phi}}\left\{\left(\mp 1 + \frac{1}{\sin\Phi}\right) e^{2ika \sin\Phi - i\frac{\pi}{4}} + \right.$$

$$\left. + \left(\mp 1 - \frac{1}{\sin\Phi}\right) e^{-2ika \sin\Phi + i\frac{\pi}{4}}\right\} . \qquad (5.9)$$

Because of the axial caustic (where an infinity of rays come together) this first order expression for the backscattered field at wide angles cannot be carried over to axial incidence without the incorporation of a caustic correction, and though the form of the wide angle result naturally suggests the use of Bessel functions, the selection of a particular Bessel function combination is not an unambiguous procedure (Ross, 1967). On the other hand, Ufimtsev (1958), using an alternative procedure based on an "asymptotic approximation" to the surface rather than the far field, has provided a first order expression for the backscattered field that is uniform in angle and in agreement with both the wide angle and on-axis formulae obtained from the geometrical theory, viz.

$$S_{V,H} \sim \frac{i}{2}\, ka \left\{\frac{J_1(2ka \sin\Phi)}{\sin\Phi} \mp i\, J_2(2ka \sin\Phi)\right\} . \qquad (5.10)$$

The cross sections computed from this expression agree reasonably well with measured data for ka of order 10, but the formula fails to reproduce some of the finer structure in the measured patterns, particularly at wider angles, and the discrepancies are quite evident when (5.10) is used to predict the cross polarized contribution to the scattering.

In order to improve the agreement it was deemed necessary to seek the second order contribution to the scattering for non-axial incidence, which terms would then serve to refine the Ufimtsev formula (5.10). In view of the solution obtained by Ross (1966) for the similar problem of a rectangular plate, it was felt

that the general form of the second order terms for wide angle scattering could be predicted: in particular, it was expected that for the vertically polarized case (electric vector parallel to the plane of the disk) the second order term would be identically zero. When the geometrical theory of diffraction was applied to the disk to obtain the second order contribution to the scattering, the result for H-polarization was as anticipated, and the two 'main' flash points did yield a zero contribution of the second order to the vertically polarized solution. But in this latter case, two additional flash points were found whose positions on the rim are functions of the angle of incidence, Φ, and these 'migrating' flash points provide a non-zero contribution. It would appear that in all previous studies of oblique scattering by circular edges, only the second order contribution arising from the interaction between the flash points P_1 and P_2 (see Fig. 5-4) has been entertained, and that the rays doubly diffracted at the migrating points P_3 and P_4 are here included for the first time.

Using the geometric theory the second order contribution to S_H produced by double diffraction at P_1 and P_2 has been found to be

$$S_H^{II} = - \frac{e^{2ika}}{\pi \sin \Phi \cos \Phi} \quad . \tag{5.11}$$

The rays doubly diffracted at P_3 and P_4, whose azimuthal angle ϕ is

$$\phi = - \cos^{-1} \frac{1}{\sqrt{1 + \sin^2 \Phi}} \quad , \tag{5.12}$$

contribute only to S_V, and their contribution can be shown to be

$$S_V^{II} = \frac{i e^{2ika\sqrt{1 + \sin^2 \Phi}}}{\pi \sin \Phi \sqrt{1 + \sin^2 \Phi}} \quad . \tag{5.13}$$

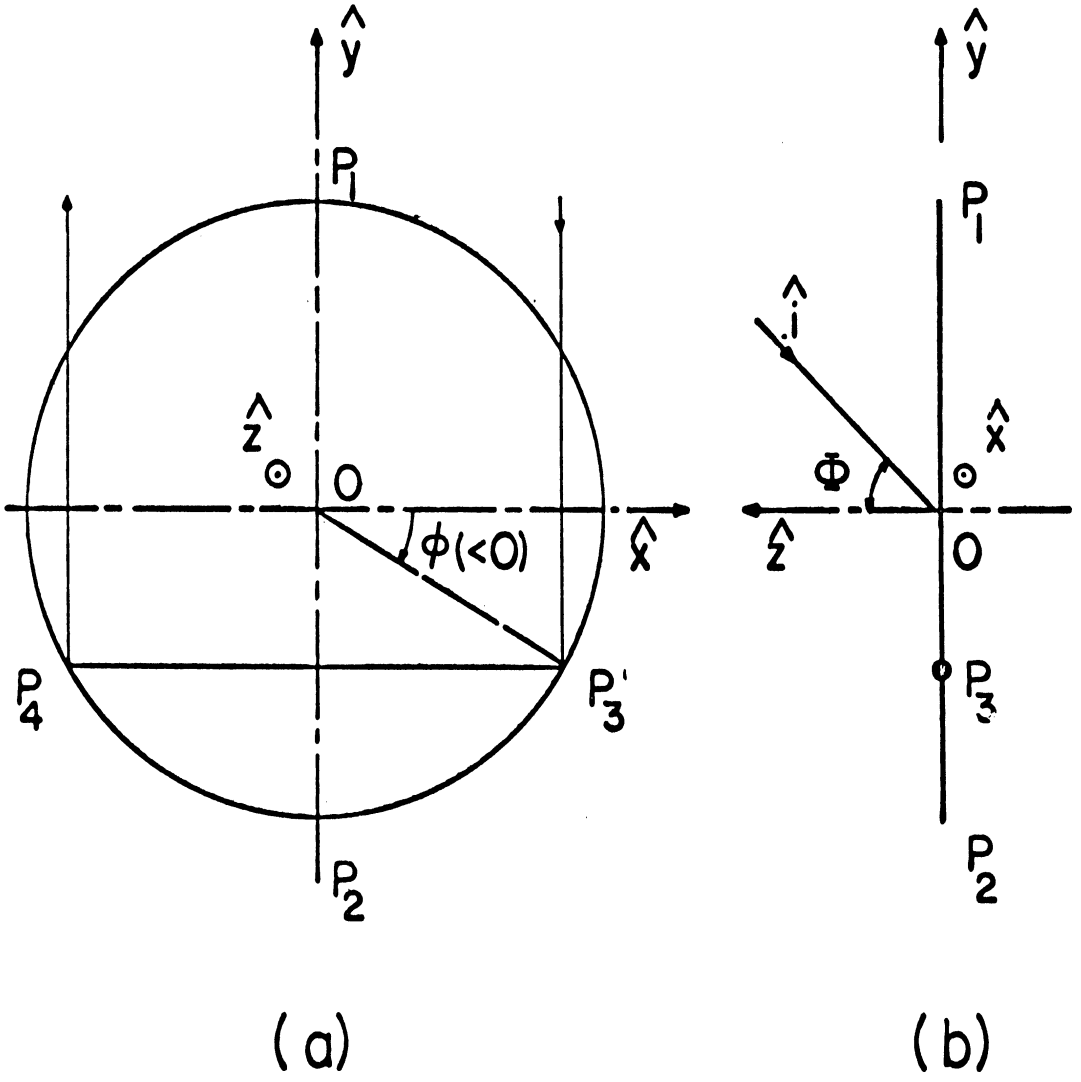

FIG. 5-4: Geometry of the scattering problem (a) in the plane of the disk and (b) in the plane of incidence.

Here again, however, it is not possible to recover the second order contribution on axis by merely putting $\Phi = 0$ in (5.11) and (5.13) because of the axial caustic, and in order to obtain an asymptotic expansion valid uniformly in Φ, it is necessary to introduce some interpolating functions which yield the on-axis ($\Phi = 0$) and off-axis (Φ bounded away from zero) formulae as particular cases.

A clue to the choice of interpolating function is provided by the works of Bowman (1970) and Weinstein (1969), and based on their studies of scattering by open waveguides we postulate that

$$S_V^{II} = -\frac{1}{2}\sqrt{\frac{ka}{\pi}}\,\frac{e^{2ika\sqrt{1+\sin^2\Phi} - i\frac{\pi}{4}}}{\sqrt{1+\sin^2\Phi}}\,M^*\left(\frac{1}{2}\sqrt{ka}\sin\Phi\right) \tag{5.14}$$

$$S_H^{II} = -\frac{1}{2}\sqrt{\frac{ka}{\pi}}\,\frac{e^{2ika - i\frac{\pi}{4}}}{\cos\Phi}\,M\left(\frac{1}{2}\sqrt{ka}\sin\Phi\right) \tag{5.15}$$

where the asterisk denotes the complex conjugate, and M (x) is related to the Fresnel integral F(x) by

$$M(x) = \frac{2}{\sqrt{\pi}}\,e^{-ix^2 - i\frac{\pi}{4}} \qquad F(x) = \frac{2}{\sqrt{\pi}}\,e^{-i\frac{\pi}{4}}\int_x^\infty e^{i(y^2-x^2)}\,dy\ . \tag{5.16}$$

We observe that (5.14) and (5.15) reduce to (5.13) and (5.11) respectively for $\sqrt{ka}\sin\Phi >> 1$, and are also consistent with the second term in (5.8) when $\Phi = 0$.

The second order expression for the backscattered field valid at all angles away from grazing ($\Phi = \pi/2$) is now

$$S_{V,H} = S_{V,H}^{I} + S_{V,H}^{II} \tag{5.17}$$

where $S_{V,H}^{I}$ is the first order contribution given in Eq. (5.10), and S_V^{II}, S_H^{II} are the second order terms given in Eqs. (5.14) and (5,15) respectively. For a more complete

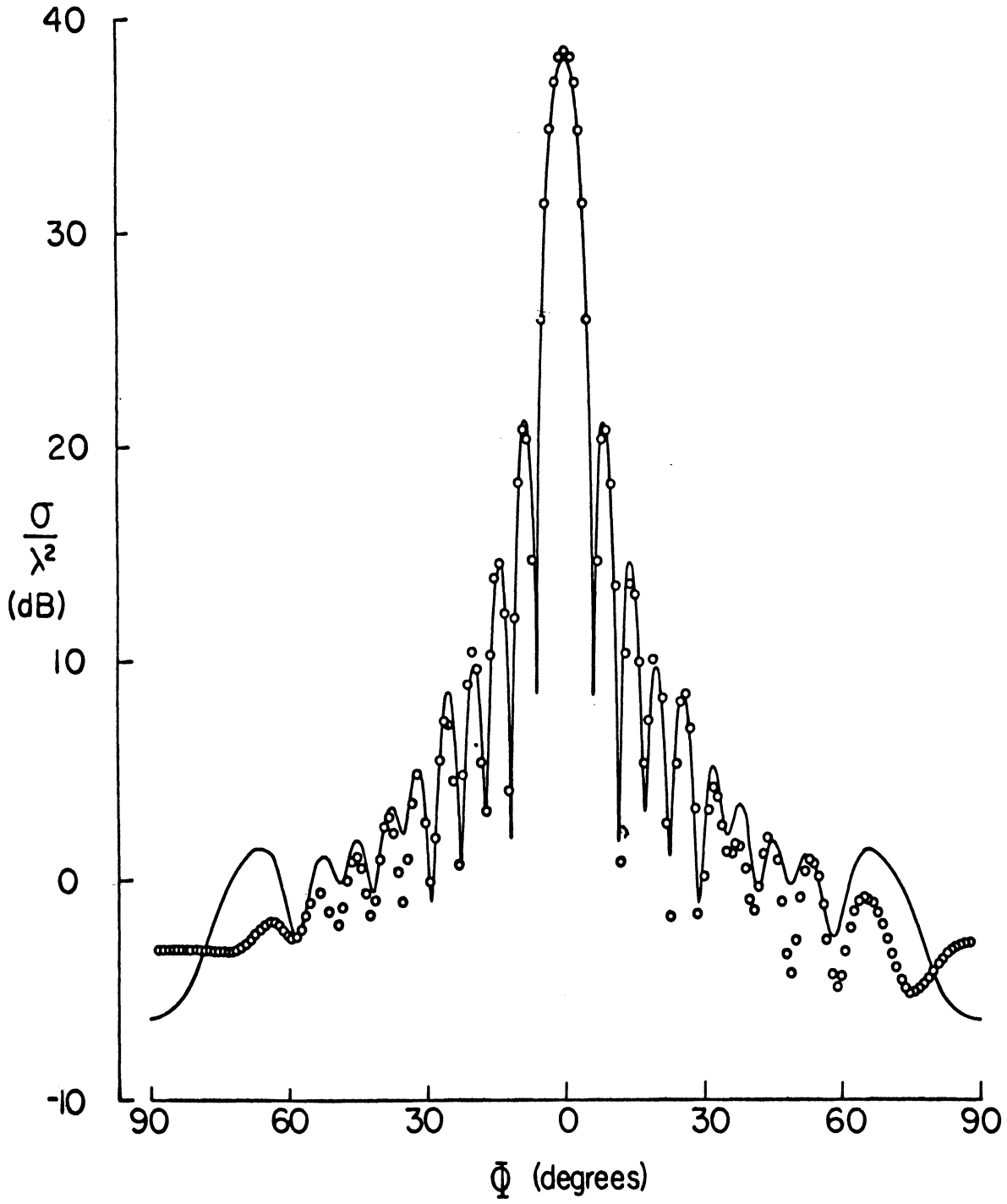

FIG. 5-5: Comparison of theory (ooo) with experiment (——) for V polarization with ka = 17.155: first order theory on left, second order theory on right.

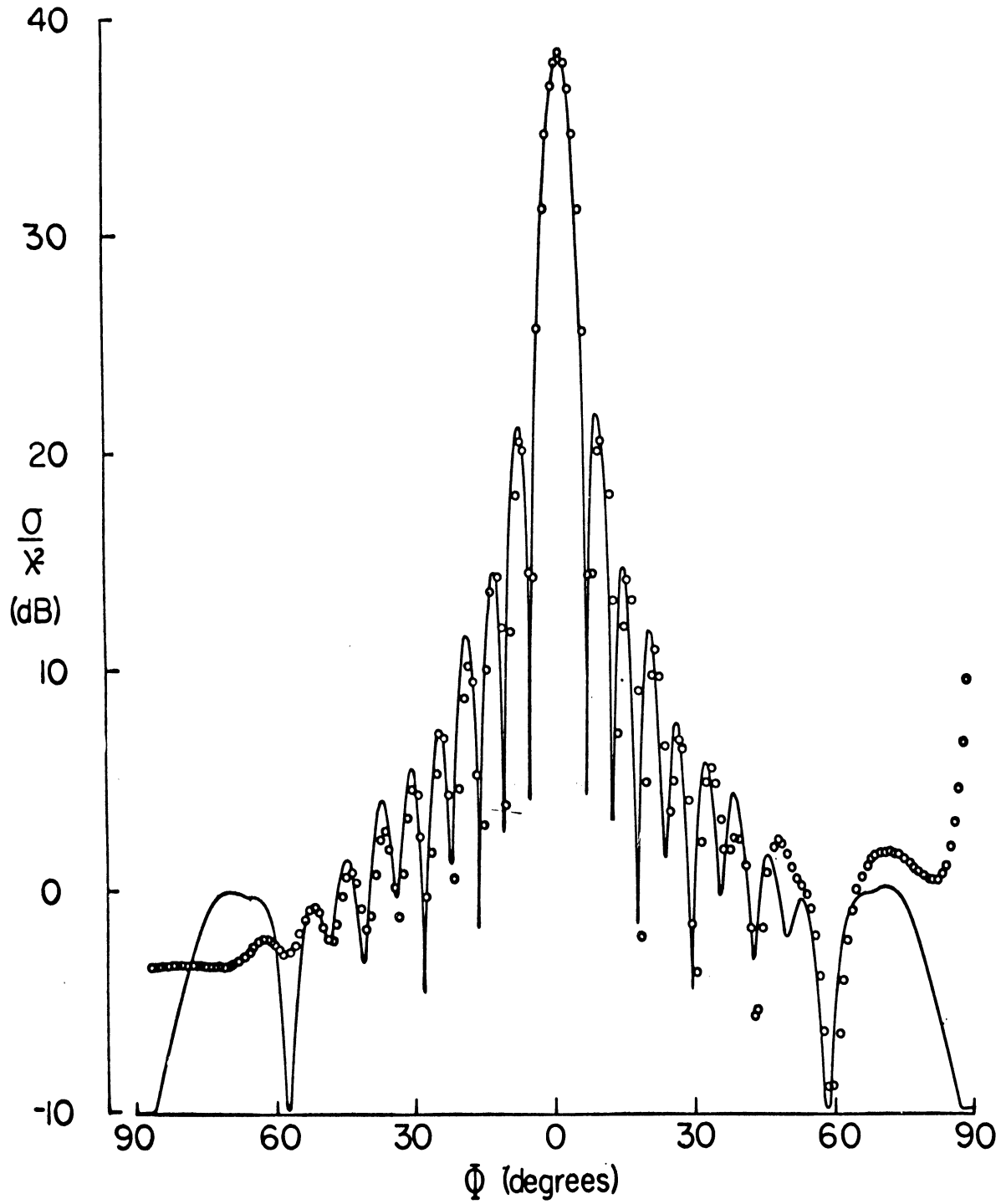

FIG. 5-6: **Comparison of theory (o o o) with experiment (——) for H polarization** with ka = 17.155: first order theory on left, second order theory on **right.**

description of the analyses leading up to this expression reference should be made to Knott et al (1970), but some idea of the accuracy of (5.17) can be obtained from Figs. 5-5 and 5-6 in which the cross sections σ_V/λ^2 and σ_H/λ^2 computed from (5.17) for ka = 17.155 are compared with experimental data. The agreement is excellent even out to $\Phi = 60^o$.

5.3 Cones

Consider a right circular (flat-backed) cone of base radius a and half-cone (included) angle γ. As before, our concern is with the far zone back scattered field when a plane wave is incident at an angle Φ to the axis of the body, and we shall distinguish two cases according as the angle Φ is measured in the plane perpendicular or parallel to the incident electric vector (denoted by subscripts V and H, respectively). But in contrast to the disk, the cone scattering problem has no known analytic solution, and our attention is therefore directed at the development of adequate asymptotic solutions with particular reference to aspect angles within the backward cone ($\Phi < \gamma$).

For axial incidence, the geometrical theory of diffraction gives (Keller, 1960)

$$S_{V,H} \sim - ka\, B(0) - \sqrt{\frac{ka}{\pi}}\, D(0)\, e^{2ika - i\frac{\pi}{4}} , \tag{5.18}$$

where

$$B(0) = (2n \sin \frac{2\pi}{n})^{-1} \tag{5.19}$$

$$D(0) = \left(\frac{\frac{1}{n} \sin \frac{\pi}{n}}{\cos \frac{\pi}{n} - \cos \frac{3\pi}{2n}} \right)^2 \tag{5.20}$$

with $n = \frac{3}{2} + \frac{\gamma}{\pi}$. The first term on the right hand side of Eq. (5.18) is produced by direct scatter from every element of the ring singularity at the base of the cone (first order contribution), whereas the second term is produced by primary interaction between all diametrically opposed elements of the ring (second order contribution).

For incidence away from axial but still within the backward cone, Keller (1960; see, however, Bechtel, 1965) has generated only the first order solution, and this is

$$S_{V,H} \sim -\frac{\sin\frac{\pi}{n}}{2n}\sqrt{\frac{ka}{\pi \sin\Phi}}\left\{\left[\mp(\cos\frac{\pi}{n}-1)^{-1}+\left(\cos\frac{\pi}{n}-\cos\frac{2(\gamma-\Phi)}{n}\right)^{-1}\right]e^{i\xi - i\pi/4}\right.$$

$$\left.+\left[\mp(\cos\frac{\pi}{n}-1)^{-1}+\left(\cos\frac{\pi}{n}-\cos\frac{2(\gamma+\Phi)}{n}\right)\right]^{-1}e^{-i\xi+i\pi/4}\right\} \qquad (5.21)$$

with

$$\xi = 2ka \sin\Phi \ . \qquad (5.22)$$

The expression in Eq. (5.21) becomes infinite as $\Phi \to 0$ as a consequence of the axial caustic, and it is again necessary to seek interpolating functions which will match (5.21) to the first term of (5.18). Although the nature of these functions has been the subject of some debate (see, for example, Ryan and Peters, 1969, 1970), these are specified if we impose the simple and obvious requirement that the resulting expression reduce to the disk result (5.10) on putting n = 2. We then have

$$S_{V,H} \sim -ka\left\{\pm A J_2(\xi) + B(\Phi) J_0(\xi) - i\,C(\Phi) J_1(\xi)\right\}, \qquad (5.23)$$

valid for $0 \le \Phi < \gamma$, where

$$A = \frac{\frac{1}{n}\sin\frac{\pi}{n}}{1-\cos\frac{\pi}{n}} \qquad \text{(independent of } \Phi\text{)}, \qquad (5.24)$$

$$B(\Phi) = \frac{\sin\frac{\pi}{n}}{2n}\left\{\frac{1}{\cos\frac{\pi}{n} - \cos\frac{3\pi-2\Phi}{n}} + \frac{1}{\cos\frac{\pi}{n} - \cos\frac{3\pi+2\Phi}{n}}\right\}, \tag{5.25}$$

$$C(\Phi) = \frac{\sin\frac{\pi}{n}}{2n}\left\{\frac{1}{\cos\frac{\pi}{n} - \cos\frac{3\pi-2\Phi}{n}} - \frac{1}{\cos\frac{\pi}{n} - \cos\frac{3\pi+2\Phi}{n}}\right\}. \tag{5.26}$$

Eq. (5.21) is recovered on replacing each Bessel function by the leading term in its asymptotic expansion for large ξ, and (5.23) patently reduces to the leading (first order) term in (5.18) on putting $\Phi = 0$. Equation (5.23) also reduces to (5.10) when $n = 2$ and is similar to that suggested by Ross (1967). However, Ross has approximated $B(\Phi)$ and $C(\Phi)$ for small Φ with $n \neq 2$, and since this expansion is invalid for γ near $\pi/2$, he has thereby cut himself off from the information provided by the simple disk problem.

Equation (5.23) provides a uniform first order expression for the far field amplitudes when $\Phi < \gamma$, but in order to reproduce some of the finer structure in the measured patterns, it is necessary to proceed to at least the second order. The second order contribution on axis is given by the second term in (5.18). By using the geometric theory we have succeeded in showing that for wide angles, but within the backward cone, the second order contribution to S_H is

$$S_H^{II} = -\frac{e^{2ika}}{\pi \sin\Phi} D(\Phi) \tag{5.27}$$

where

$$D(\Phi) = \frac{\frac{1}{2}\sin^2\frac{\pi}{n}}{n\left(\cos\frac{\pi}{n} - \cos\frac{3\pi-2\phi}{2n}\right)\left(\cos\frac{\pi}{n} - \cos\frac{3\pi+2\phi}{2n}\right)} \tag{5.28}$$

and a comparison with Eq. (5.11) now shows that the caustic matching problem for this term is identical to that already faced in connection with the disk. A uniform

expression for S_H^{II} valid for $0 \leq \Phi < \gamma$ is therefore

$$S_H^{II} = -\sqrt{\frac{ka}{\pi}}\, e^{2ika - i\pi/4}\, D(\Phi)\, M\left(\frac{1}{2}\sqrt{ka}\, \sin\Phi\right) \tag{5.29}$$

where the function M(x) is defined in Eq. (5.16), and the required second order expression is

$$S_H = S_H^I + S_H^{II} \tag{5.30}$$

with S_H^I as given in Eq. (5.23). For $\gamma = 15^o$, scattering patterns computed using (5.30) have been compared with measured data. The agreement is quite good.

The analysis for vertical polarization is a little more involved, and we have not yet had time to complete the derivation of the second order contribution to S_V for wide angle scattering. We expect, however, that S_V^{II} will bear the same sort of relation to its value for a disk as does (5.27) to (5.11), with at most a coefficient different from the function $D(\Phi)$ appropriate to S_H^{II}.

We have so far considered only aspects within the backward cone, but for horizontal polarization an asymptotic approximation to S_H has been developed for all aspects out to the direction $\Phi = \frac{\pi}{2} - \gamma$ of the specular flash. Asymptotically at least, no contribution associated with the farther flash point can be obtained when $\Phi > \gamma$, and thus the first order contribution to S_H will consist only of the terms in (5.21) involving $e^{-i\xi}$ and the second order contribution will be zero. In practice, no such abrupt change in S_H is observed or could occur. As Φ increases through the value γ, those portions of S_H which we have omitted in the above will continue to be present, but with amplitudes which decrease rapidly with increasing $(\Phi - \gamma)$, and a formula which has been found effective over the entire range $0 \leq \Phi \leq \gamma$ is

$$S_H \sim S_H^I + S_H^{II} \tag{5.31}$$

with

$$S_H^I = -ka\left[AJ_2(\xi)+B(\Phi)J_0(\xi)x-i\,C(\Phi)J_1(\xi)\right.$$

$$\left.+\frac{e^{i\xi-i\,\pi/4}}{\sqrt{2\pi\xi}}\left\{A-B(\Phi)+C(\Phi)\right\}\left\{1-\Gamma(\Phi)\right\}\right]\left\{1-\tau\left(\sqrt{2kan\,\mathrm{cosec}\gamma\left|\sin\frac{2\pi-\Phi}{n}\right|}\right)\right\}, \tag{5.32}$$

$$S_H^{II} = -\sqrt{\frac{ka}{\pi}}\,e^{2ika-i\,\pi/4}\,D(\Phi)\Gamma(\Phi)\,M\left(\tfrac{1}{2}\sqrt{ka}\sin\Phi\right), \tag{5.33}$$

where

$$\tau(x) = \frac{\sqrt{\pi}}{2x}\,e^{i\pi/4}\left\{e^{-ix^2} - M(x)\right\} \tag{5.34}$$

and

$$\Gamma(\phi) = \begin{cases} 1 & 0 \le \Phi \le \gamma \\ e^{-2ka\,\sin(\Phi-\gamma)} & \gamma < \Phi \le \pi/2 - \gamma \end{cases} \tag{5.35}$$

These are three features of this result that should be pointed out. In the first place, the factor $\Gamma(\Phi)$ which, for $\Phi > \gamma$, provides an exponential decrease of all contributions from the shadowed flash point is entirely empirical. No attempt has been made to represent the 'creeping wave' decay factor which should logically appear, but the form that has been chosen was suggested by experimental data and is consistent with those measured patterns that we have examined. It will also be noted that we have retained the Bessel function combination characteristic of the backward cone out beyond $\Phi = \gamma$, but have allowed for this in (5.32) via the second group of terms. We have found this procedure necessary to avoid a discontinuity at $\Phi = \gamma$: for many cones of interest, 2ka sin γ is not sufficiently large to justify the insertion of the asymptotic formulae for the Bessel functions. Finally, we remark that in the

vicinity of the specular flash direction, the form of S_H is that obtained from a careful application of the physical optics approximation, with the matching into the caustic at $\Phi = \frac{\pi}{2} - \gamma$ being provided by the function $\{1 - \tau(x)\}$ that Senior (1967) derives.

To judge from those computations that have been made, Eq. (5.31) is an effective means of cross section estimation for the entire range $0 \leq \Phi \leq \frac{\pi}{2} - \gamma$ and is markedly superior to (and more general than) any other that has previously been published. It is our belief that only a little more effort would enable us to arrive at a corresponding result for S_V.

5.4 Experimental Work

The motivation underlying the theoretical treatments of disks and cones was to understand the role played by edges in contributing to the cross polarized echoes. The cone, of course, is of more interest in reentry phenomena because it is a shape used entirely or in part in the design of reentry bodies, but it was the disk study that led to subsequent development of the asymptotic theory for the cone. The route by which one arrives at the cross polarized scattering is via the direct scattering as declared by Eq. (5.6), and once the direct S_V and S_H scattering are found, the cross polarized return is a trivial computation.

Since there is no analytical solution to the cone problem, asymptotic approaches are natural alternatives; these techniques are approximations and it is only prudent to evaluate them by comparison with experiment. In addition to supplying a 'data base' simply as a check of the theoretical results, careful and systematic experimental work can also provide the information needed for empirical descriptions in which it is simply too difficult or too time-consuming to follow a rigorous theoretical approach. It turns out that nowhere in the literature does there exist a systematic and acceptable set of experimental cone data against which our cone results can be compared. There are, of course, scattered assortments of data, but these are too isolated and specific to be of much use. A notable collection

of systematically measured cone data does exist in Keys and Primich (1959) but unfortunately we found the patterns to be too small and of questionable accuracy; in addition, the measured cones were a bit too small to satisfy the asymptotic assumptions. There is also a collection of data such as given by Blore (1964) for a considerable range of frequency, but these are invariably for on-axis incidence and are of no use in assessing wide-angle scattering. We found no experimental phase data on cones anywhere in the literature.

Faced with such a shortage of data, especially phase data, we launched an experimental measurements program designed to collect enough data in a systematic fashion that the theory could be checked and provide information that might be useful for empirical descriptions. Our equipment is modest and phase is ordinarily measured by cancelling the received signal by a reference signal whose phase and amplitude is manually controlled. The technique is a standard one, but requires a great deal of time since the cancellation process must be performed at each and every aspect angle for which phase data are desired. To surmount this problem and yet maintain the simplicity of the equipment, we devised a novel three-trace laboratory measurement scheme (Knott, 1969) that reduced the data collection time to a tenth or less of that required by the more classic cancellation method. The time saved must be reinvested later to process the data, but the method drastically reduces range time.

We confined the measurements to a single cone target with a base diameter of 10.00 centimeters and a half cone angle of 15 degrees. A short cylindrical foamed dielectric support was cemented to the cone and a circle of slightly larger size was marked on the flat top of the main foamed dielectric support column. The circle was concentric with the column spin axis and permitted the range operator to install the cone model within .03 inch of the same position for every measurement.

Since our interest was in the region of axial incidence, cone patterns were recorded only for aspect angles of 30 degrees or less. Measurements were carried out for both horizontal and vertical polarizations and were made at 31 evenly spaced frequencies between and including 8.0 and 11.0 GHz. Since the geometrical theory of diffraction predicts that energy will flash across the shadowed base of the cone, we felt it would be of interest to include measurements of the cone with an absorbent pad mounted on its base to suppress these rays. The entire experimental program thus involved essentially two targets, two polarizations, 31 frequencies and three traces per pattern, or a total of 372 individual radar cross section traces. The quality and quantity of data are a credit to the skill and patience of the range operator and represent as fine a collection of cone scattering data as exists anywhere in the nation. Figure 5-7 is a reproduction of a typical pattern showing the three traces.

The measurements produced a stack of patterns which, when riffled by the thumb of one hand, gave the impression of a slow motion movie. Odd numbered lobes (with nose-on representing number one) of the bare cone rose and fell in unison while even numbered lobes did the reverse; this action was greatly suppressed in the patterns taken of the cone with the absorber on its base. We selected three frequencies, one each near the ends and center of the range covered, and digitized all the traces at one-degree intervals in aspect angle. This was strictly a manual process accomplished by two men simultaneously, one calling out numbers while scanning a pattern and the other, seated at a key punch, transcribing the numbers onto cards.

After processing the digitized data, we quickly saw that the phase of the horizontal and vertical returns were different, as of course they should be, but it turned out that we could not establish the relative phase of the cross-base contribution. This was because, even when the range dependence of the phase is accounted for, there is no simple way to distinguish the phase of the first order

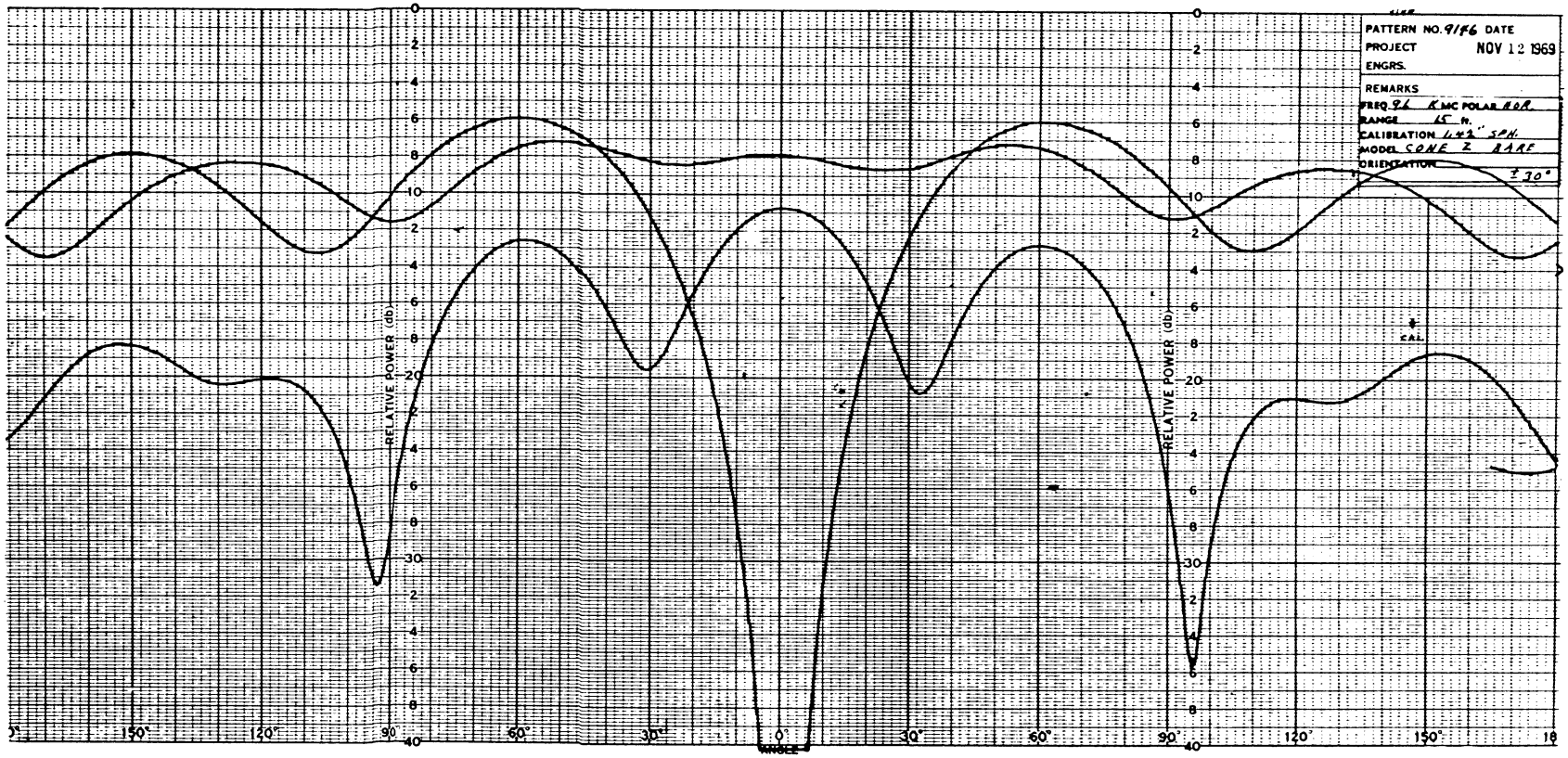

FIG. 5-7: This is a sample of typical cone data recorded in the laboratory. The trace having three prominent humps is the cone cross section pattern and the other two traces are used to obtain its phase behavior.

base returns from that of higher order (cross-base) returns. Time did not permit us to proceed any further with the phase data, but we fully intend to do so when time and funds permit.

The amplitude data from all the measurements have been digitized at one-degree intervals in aspect angle, in order to have on hand the scattering behavior both as a function of frequency and aspect angle. The typical pattern shown in Fig. 5-7 is somewhat misleading both because of the extra two traces needed to calculate phase and because of the expanded scale. Figures 5-8 and 5-9 serve to present a more usual perspective of the scattering pattern by including aspects out to 70 degrees or so. At the particular frequency chosen for these figures the horizontal pattern (Fig. 5-8) shows a pair of prominent lobes at an aspect of 10 degrees which are replaced in the vertical pattern (Fig. 5-9) by a pair of prominent nulls. It is evident that two nearly equal contributors are added together in the one case to produce a lobe and subtracted in the other to produce a null. Equation (5.21) clearly shows this mathematically by demanding plus or minus sign selections depending on polarization.

A convenient way of displaying the cone amplitude scattering data is by means of the contour diagrams of Figs. 5-10 and 5-11. Each contour line represents a constant radar cross section amplitude and for these diagrams, the contours are 2 dB apart. The horizontal data of Fig. 5-10 show a dominant lobe centered on 9.4 GHz and 10 degrees in aspect, flanked by two troughs of nulls, one centered on about 8.7 GHz and 7 degrees aspect, the other centered near 10.0 GHz and 15 degrees aspect. The diagram clearly shows that the nulls crowd closer toward nose-on incidence at the higher frequencies. Beyond an aspect of about 20 degrees, the returns are fairly uniform, marked by no strong lobe or null structure.

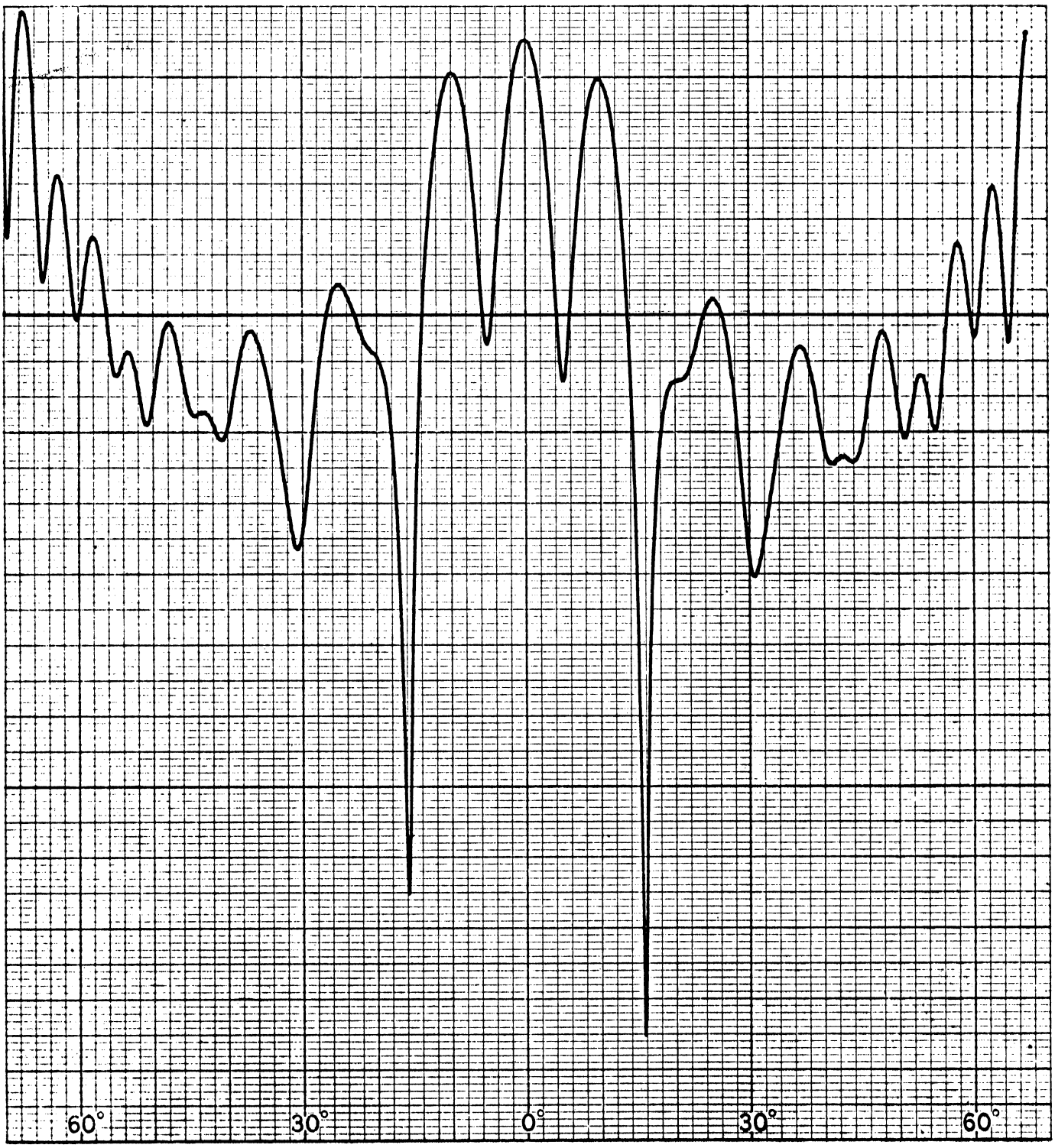

FIG. 5-8: An experimental horizontal principal plane pattern of the cone target for ka = 10 shows strong lobes at 10-degree aspect angle. The heavy horizontal line is a calibration level of one square wavelength. From top to bottom the amplitude scale covers a range of 32 dB.

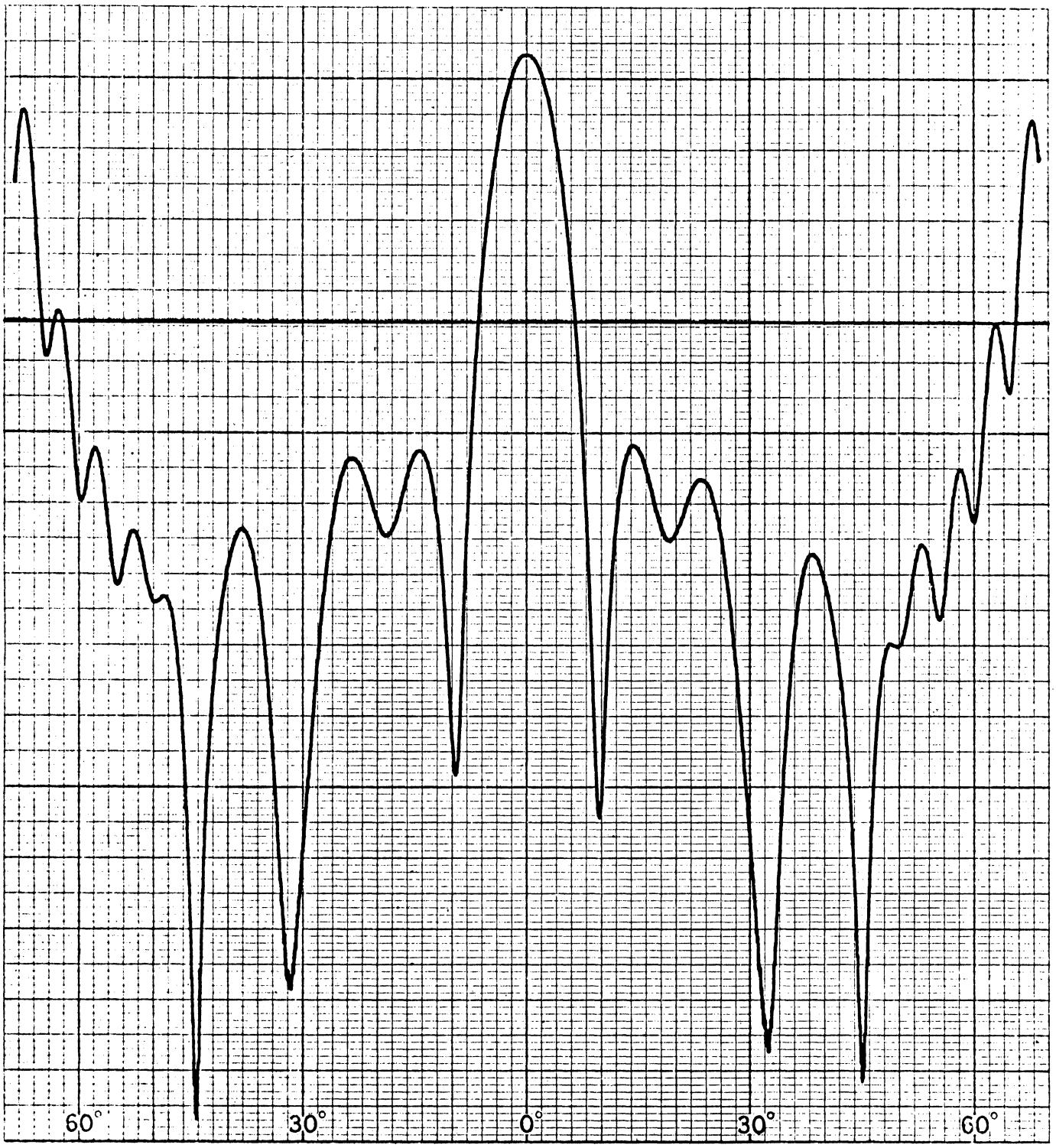

FIG. 5-9: The experimental vertical pattern of the cone shows deep nulls in the place of the first off-nose-on lobes of Fig. 5-8.

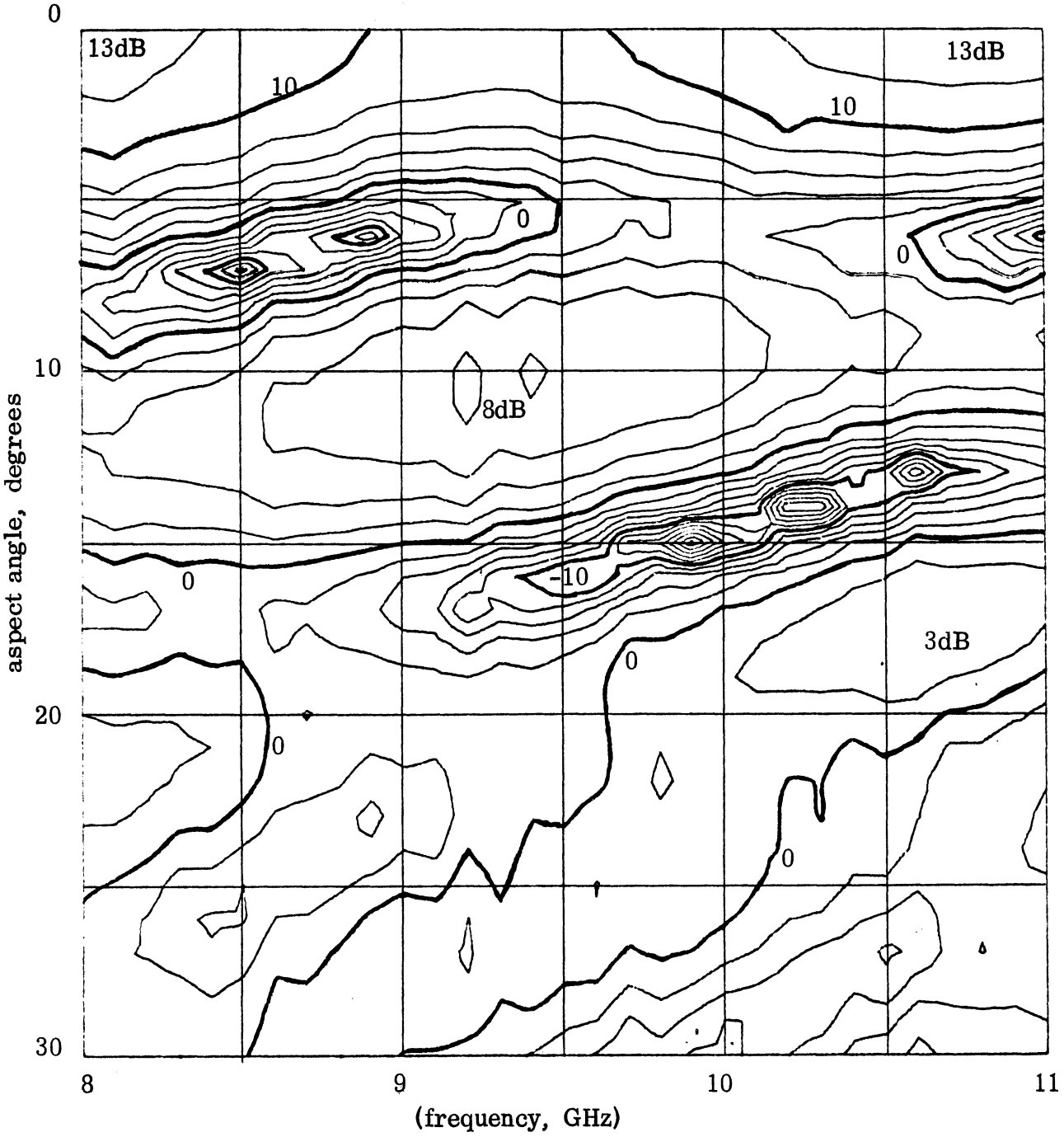

FIG. 5-10: Horizontal cone returns show a dominant lobe centered on 9.4 GHz and 10 degrees aspect; a less intense lobe lies at 10.6 GHz and 17 degrees. Note the troughs of deep nulls lying between lobes.

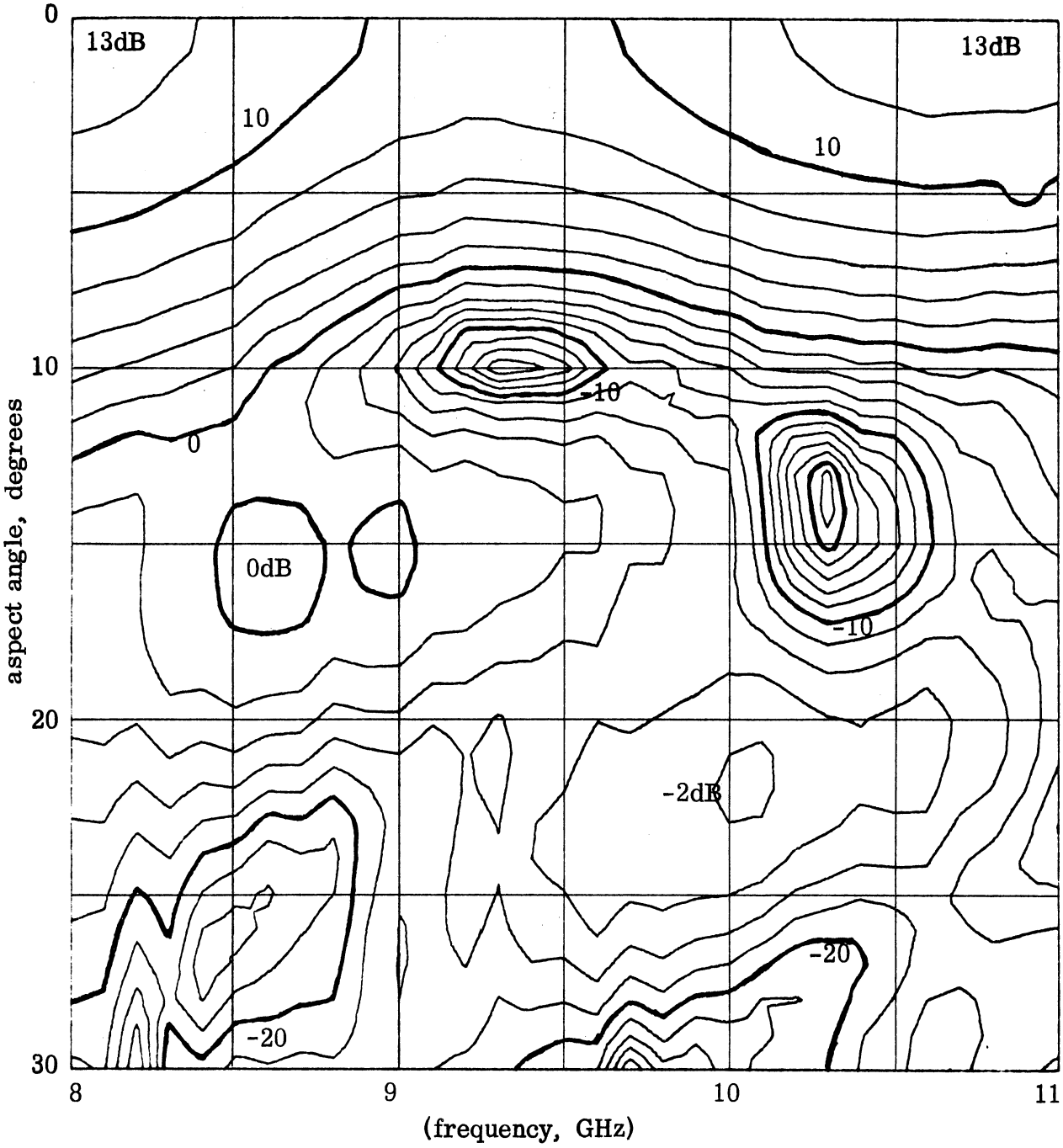

FIG. 5-11: Vertical cone returns show deep nulls at 9.4 GHz, 10 degrees and 10.3 GHz, 14 degrees. Beyond 20 degrees aspect the returns are very low.

The vertical returns are shown in Fig. 5-11 and the dominant lobe in the horizontal returns (at 9.4 GHz and 10 degrees aspect) has been replaced by a deep null. A deep null also appears that 10.3 GHz and 14 degrees and a pair of modest lobes appear at 8.6 GHz, 15 degrees and 10.1 GHz, 22 degrees. The vertical cone patterns have broader lobes in the nose-on region than the horizontal patterns, and beyond the half cone angle the returns are a magnitude or more smaller.

A theoretical diagram of the horizontal cone scattering is shown in Fig. 5-12 based on the prescription given by Eqs. (5.23) and (5.27). Note that the positions of the dominant lobes are correctly predicted, but that the amplitudes tend to be too high. One reason for this is that for cones this size higher order contributions are not negligible; another is that the empirical factor Γ of Eq. (5.35) was not used in the calculation beyond the cone angle (15 degrees) so that the amplitude of the lobe lying at 10.7 GHz and 18 degrees has not been suppressed as the experimental data suggest it should be. Nontheless, the theory now estimates cone scattering more effectively than has been possible in the past.

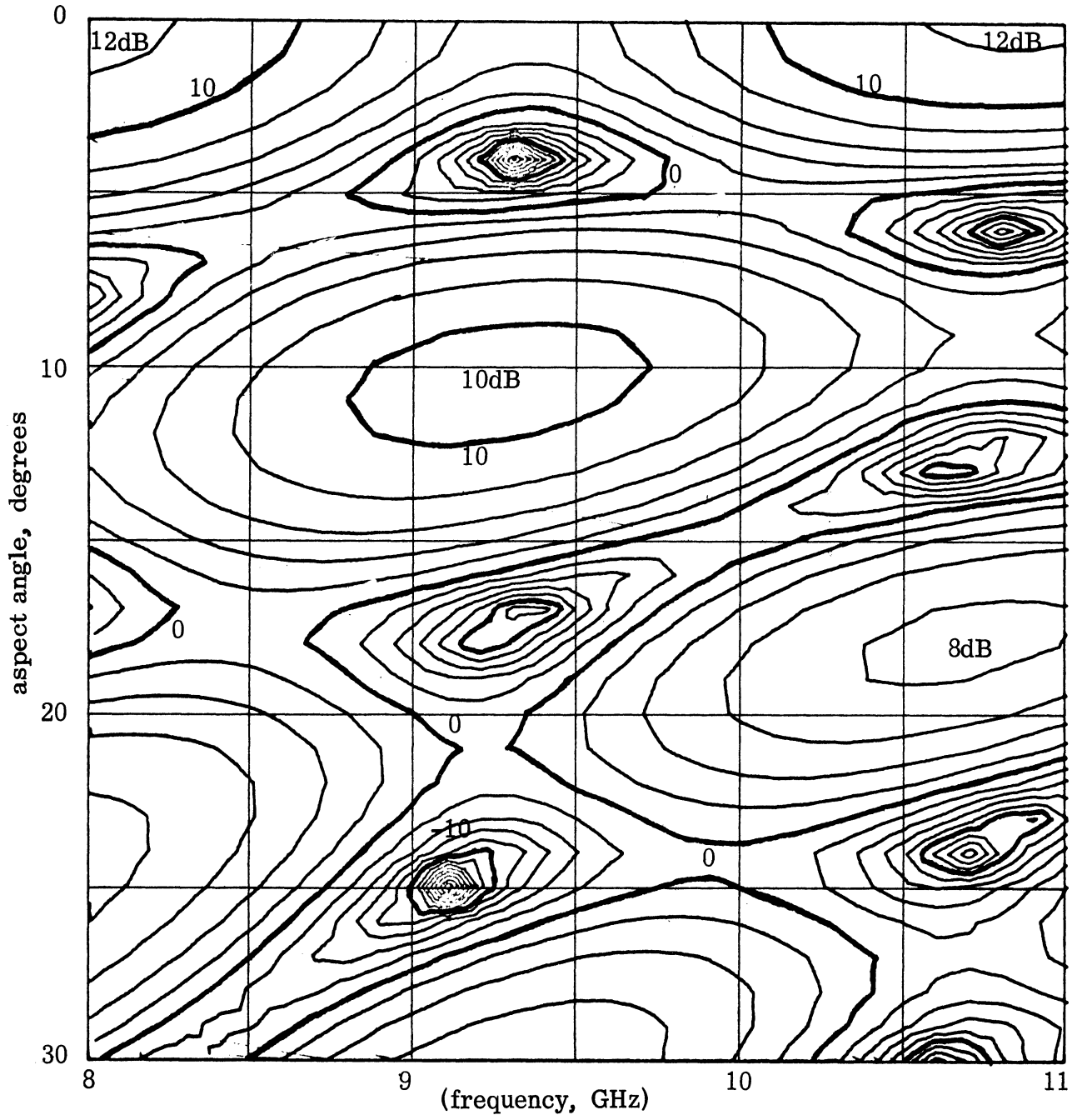

FIG. 5-12: Theoretical contour diagram for the horizontal returns requires at least second order terms to produce the dominant lobe seen in the experimental data. Locations of the lobes were correctly computed, but the amplitudes are somewhat higher than measured.

VI

SUMMARY AND CONCLUSIONS

It is clear to us that the cross-polarized capability of the ARIS has been one of its important, but heretofore neglected, signature measurements. We have proposed and tested a five-parameter method of instrumentation and analysis that exploits the best features of both coherent and non-coherent radars; it is our firm belief that ARIS and the users of ARIS data can benefit from this concept if it is implemented. We therefore recommend that

1) The feasibility of instrumenting the five-parameter method be studied; the required equipment is conceptually simple and inexpensive.

2) Given a body polarization angle history, it appears that body aspect angle can be deduced. The paper study of Chapter III involved only circular precession and further studies of more general cases (i.e. elliptical precession and planar oscillations) ought to be pursued.

3) The theoretical study of cone scattering (Chapter V) has paved the way for a more detailed treatment of flared objects with convex terminations on the base of the body; the treatment of such terminations is not trivial, and should be approached with with intent of defining more explicitly the cross polarized returns.

This Appendix is Unclassified

APPENDIX A

Summary of The University of Michigan Radiation Laboratory Reports on ARIS Data

In this appendix we list the title of each chapter of each report issued during the two contract efforts. Beneath each chapter title, unless the title is self-evident, appears a terse statement in parentheses describing the essential content of the chapter. The intent of the presentation is to display in abbreviated form the location of topics the reader might choose to examine in detail. It is also a means of summarizing the past 38 months of research on ARIS data.

Each report is summarized on a single page. Although the first four were issued under a different contract than the last two, all six are treated as a single series of documents.

The University of Michigan delivered copies of each issue in batch form to the Director of Range Engineering (ETEQO), who handled the subsequent distribution; the number of documents in each batch ranged from 10 to 25. All are classified Group 1 - "Excluded from Automatic Downgrading Provisions", but the report titles, chapter titles, and summary descriptions in this Appendix are unclassified.

FIRST REPORT: Interim Report No. 1, Contract F08606-67-C-0071

"Analysis of ARIS Data Gathering and Extraction Methods"

Report Number: 8798-1-T
Author: Ronal W. Larson
Date: 15 November 1967

I. INTRODUCTION
(The research goal is defined as "utilizing presently available ARIS radar data to obtain methods for determining the size and shape of reentry vehicles".)

II. GEOMETRY OF REENTRY
(The polarization angle is defined by the relations between the velocity vector, the line of sight, and the target axis.)

III. RECEIVED SIGNALS
(The received signals are expressed in terms of the principal plane target backscattering patterns.)

IV. INVERSE SCATTERING
(ARIS data in principle can lead to two or three body parameters.)

V. LABORATORY MEASUREMENTS
(Measurements of non-principal plane patterns helped explain some features of ARIS data.)

VI. SIZING OF H0013 DATA

VII. COMPUTER SIMULATION
(Theoretical returns from cylinders are programmed.)

VIII. FUTURE WORK

SECOND REPORT: Interim Report No. 2, Contract F08606-67-C-0071

"Analysis of Methods of Gathering and Interpreting ARIS Data"

Report Number: 8798-2-T
Authors: Ronal W. Larson, E.F.Knott, and T.M.Smith
Date: 1 May 1968

I. INTRODUCTION

II. BASIC RELATIONSHIPS
(Reentry geometry and received signals are studied in more detail.)

III. LABORATORY EXPERIMENTS
(Measurements verify that cross polarized returns are derivable from principal plane scattering data; a mechanical precession simulator is described and data acquired with it are interpreted.)

IV. COMPUTER SIMULATIONS
(The computer is used to generate theoretical returns for a roll-symmetric target and the resulting data analyzed as if they were signature data; emphasis is on the cross polarized data as a way of deducing target motion.)

V. PLASMA PHENOMENA
(A theoretical plasma-capped sphere model produces behavior comparable to actual observations.)

VI. ANOMALOUS EDGE SCATTERING
(A theoretical treatment of an infinite strip initiates the study of edges in scattering.)

VII. ANALYSIS OF RECENT TESTS
(A step-by-step analysis of Test H0028 is presented on endo-atmospheric data; evidence of a specific vehicle feature predicted by other agencies was completely lacking.)

VIII. CONCLUSIONS AND PLANS FOR FUTURE WORK

THIRD REPORT: Interim Report No. 3, Contract F08606-67-C-0071

"Analysis of Methods of Gathering and Interpreting ARIS Data"

Report Number: 8798-3-T
Author: Eugene F. Knott
Date: January 1969

I. INVERSE SCATTERING
(The real problem is not inverse scattering, per se, but the recovery of a principal plane pattern on which to operate.)

II. STUDIES OF BODY MOTION
(Motion of a spinning vehicle is qualitatively derived for small angles of attack.)

III. CONTINUED STUDIES OF SPECIFIC MISSIONS
(Segments of the exo-atmospheric principal plane patterns from one test flight are extracted and the cross polarized endo-atmospheric data from another are used to estimate target orientation.)

IV. PLASMA PHENOMENA
(Previous treatment is expanded and compared with typical flights.)

V. EDGE SCATTERING AND CROSS POLARIZED CALIBRATION
(Strip theory is pursued and applications to cone configuration is postulated; cross polarized calibration is complicated by the inevitable orientation sensitivity of any calibration standard.)

VI. USES OF THE COMPUTER
(Pattern recognition and the Stromberg-Carlson 4020 system are discussed as analysis and research tools.)

VII. CONCLUSIONS

FOURTH REPORT: Interim Report No. 4, Contract F08606-67-C-0071

"Analysis of Methods of Gathering and Interpreting ARIS Data"

Report Number: 8798-4-T
Authors: E.F.Knott, A.G.Cole, K.M.Jagdmann, and G.R.Mattson
Date: April 1969

I. INTRODUCTION

II. BODY MOTION
(Results of the previous derivation are interpreted for exo-atmospheric and endo-atmospheric portions of reentry.)

III. CROSS POLARIZED RADAR RETURNS
(Theoretical and experimental results lead to the development of a sizing scheme that exploits the cross polarized exo-atmospheric returns.)

IV. DISK SCATTERING
(A theoretical treatment of the disk is intended to give some insight to the more practical case of the cone.)

V. PATTERN RECOGNITION
(A scheme based on theoretically generated signature data correctly differentiated a sphere-tipped cone from a sharply tipped cone.)

VI. SPECIFIC TEST ANALYSES
(Signatures were successfully simulated for one test, the vehicle of another test was sized, and the study of a third test was concluded.)

VII. CONCLUSIONS AND RECOMMENDATIONS

FIFTH REPORT: Interim Report No. 1, Contract F08606-69-C-0045

"Analysis of ARIS Data"

Report Number: 2649-1-T
Author: Eugene F. Knott
Date: December 1969

I. THE ROLE OF ARIS IN RADAR TARGET SIZING
(Three ways to acquire more target data are discussed; two of them appear impractical, but the third is promising.)

II. EXPERIMENTAL TESTS
(An experiment designed to test the feasibility of the third method verified the concept; unintentional experimental oversights showed that the system cannot be fooled.)

III. CONSTRUCTING LIBRARIES OF PATTERNS
(Before libraries can be assembled, better theoretical descriptions and more accurate target dimensions are needed.)

IV. TEST H0037
(The signature data for the vehicle show some unusual behavior; the exo-atmospheric data are studied in detail.)

V. MISCELLANEOUS TOPICS
(A small hardware problem is described along with two other minor topics.)

VI. SUMMARY AND CONCLUSIONS

SIXTH REPORT: Final Report No. 1, Contract F08606-69-C-0045

"Analysis of ARIS Data"

Report Number: 02649-1-F Volumes 1 and 2.
Authors: E. F. Knott and T.B.A.Senior
Date: June, 1970

I. SUMMARY OF RESEARCH
(Major contributions over the last 38 months of two contract efforts are summarized.)

II. THE FIVE-PARAMETER SIZING; A SEQUEL
(A final laboratory test of the five-parameter scheme explains previous experimental problems and demonstrates the desirability of instrumenting the scheme on ARIS.)

III. POLARIZATION AND ASPECT ANGLES
(A promising study shows that true aspect angle can be related to true polarization angle by means of time derivatives.)

IV. THE H0037, H0039, and H0041 TRIAD (U)
(Three similar test missions are discussed.) This appears as Volume 2 to this Final Report and is Classified SECRET.

V. SCATTERING FROM DISKS AND CONES
(A summary of the results of theoretical and experimental scattering from disks and cones is given.)

VI. CONCLUSIONS AND RECOMMENDATIONS

This Appendix is Unclassified

APPENDIX B

Many of the formulas used in signature analysis, unlike those of Chapter V, are extremely simple, but they are used so often that it saves a great deal of time to have them displayed in graphical form. Four charts are given in this appendix which we have used many times.

The first and simplest is the direct return from a conducting sphere and the second is the cross polarized return from a right circular cone. These charts are based on geometric optics theory and thus assume that typical target dimensions are much greater than the incident wavelength.

The third and fourth charts are based on the formula for the radar cross section of a cylinder and are tailored to the frequencies typically used by ARIS. The formula is

$$\sigma = \frac{\pi d \ell^2}{\lambda} \tag{B.1}$$

and if d is interpreted to be mean diameter, and ℓ to be the length of a slanted surface, the formula also works well for cone frusta. Equation (B.1) should only be used for the specular return of a surface that is large compared with the wavelength; since (B.1) is a physical optics description, the formula makes no distinction between polarizations. Nor does it account for the presence, if any, of lossy coatings on the surface of the target.

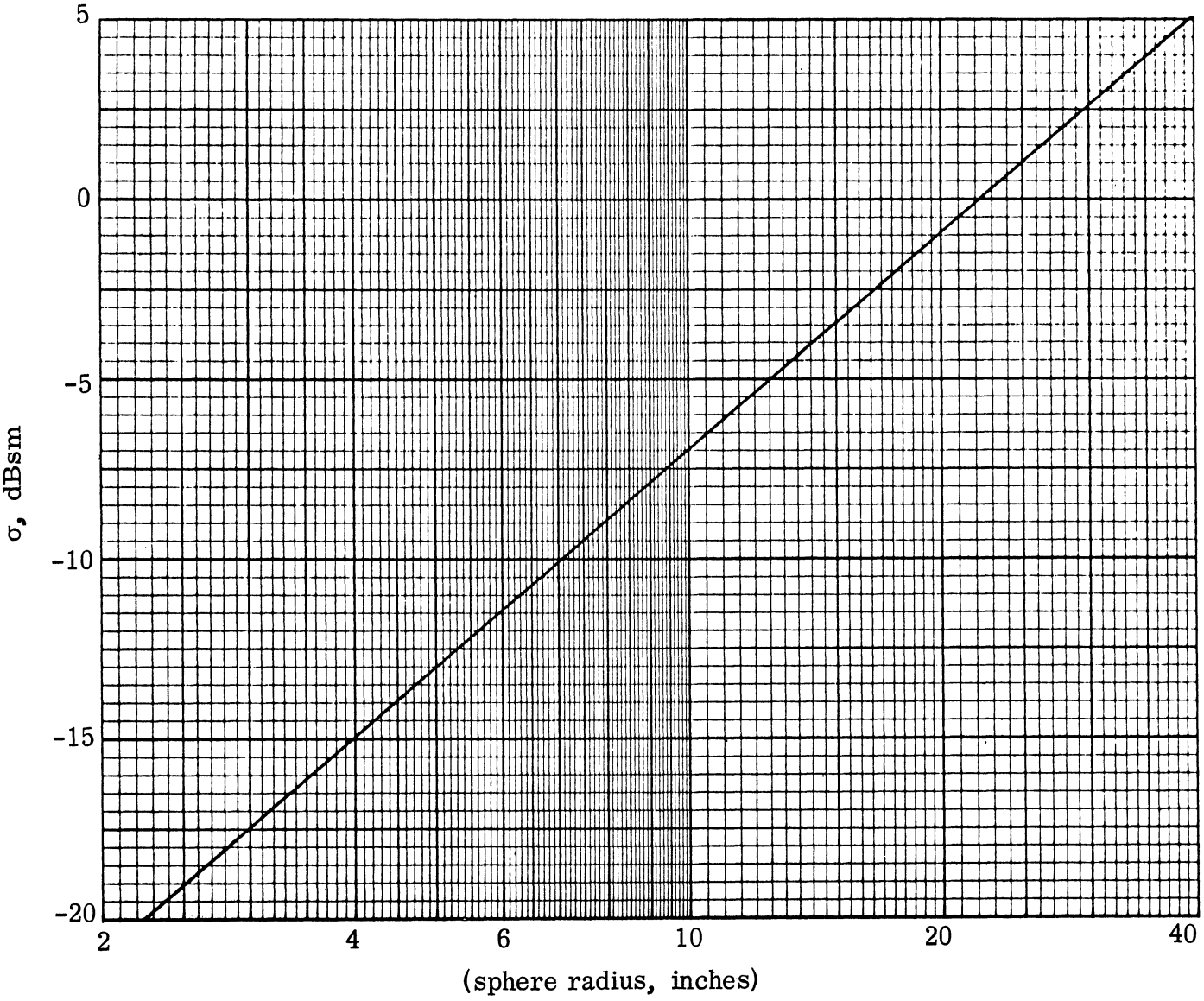

FIG. B-1: The solid line above traces out the geometric optics return of a metallic sphere. The formula is

$$\sigma = \pi a^2$$

and assumes that the sphere is much larger than the incident wavelength. The lower left extreme of the curve is thus useful only if the frequency is high enough.

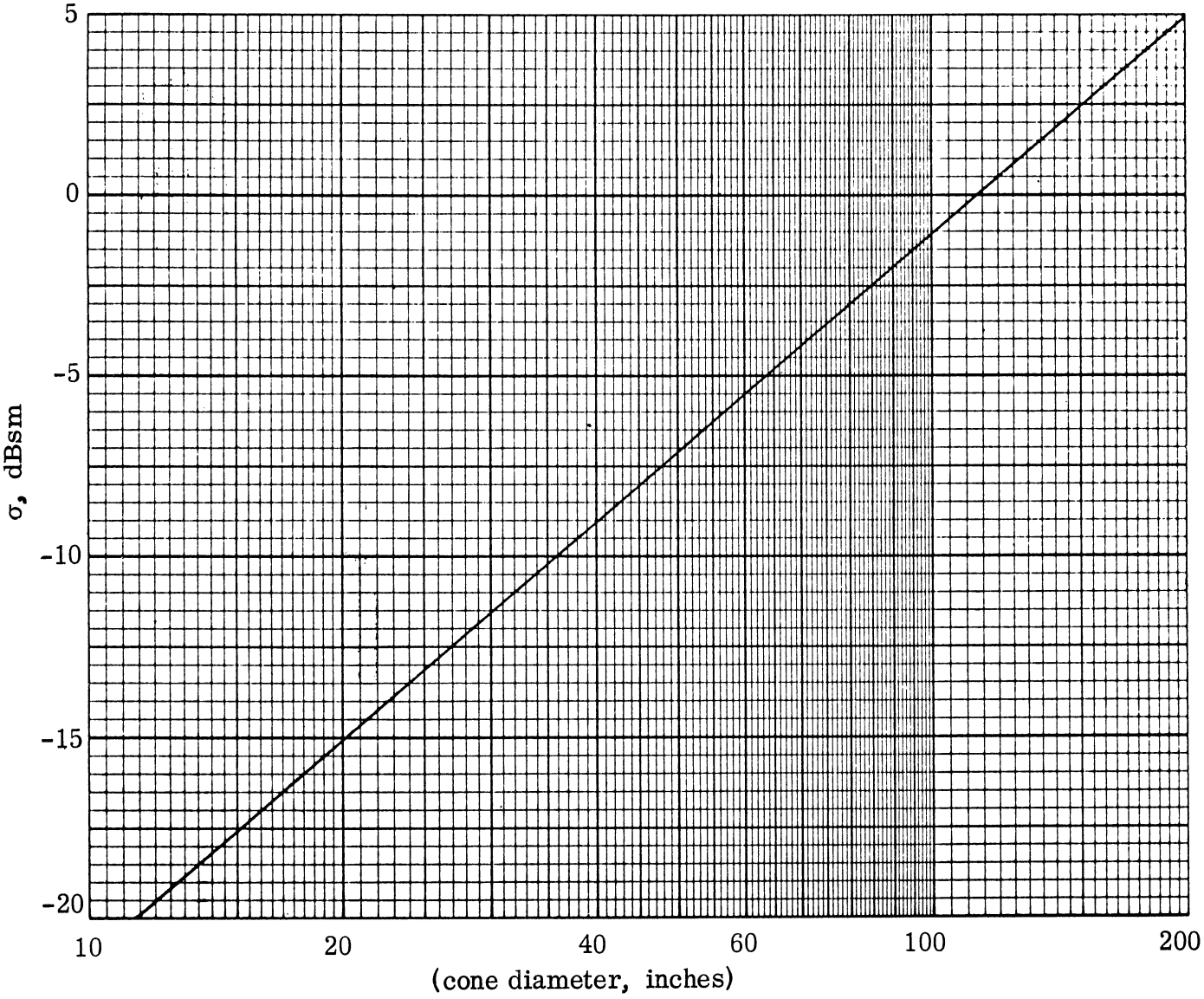

FIG. B-2: The solid line gives the maximum cross polarized return of a metallic right circular cone in the nose-on region. The formula is

$$\sigma = .1213\ d^2$$

and is accurate within $\pm$ 0.2 dB if the cone half angle is between 5 and 15 degrees. Since the formula is based on the geometric theory of edge diffraction, the base diameter must be large compared with the incident wavelength.

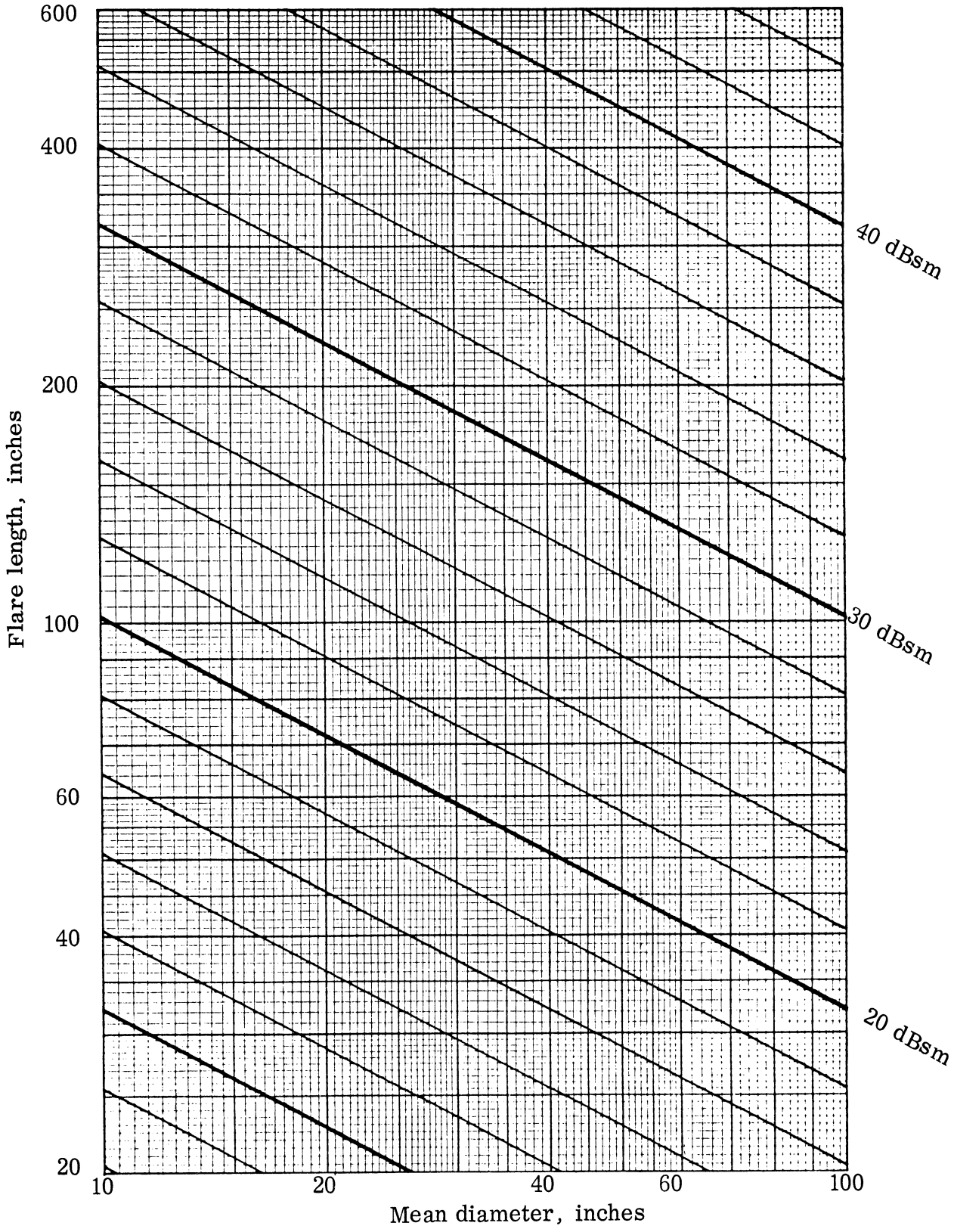

FIG. B-3: The specular radar return of a cylinder or cone frustum can be found from this C-band chart.

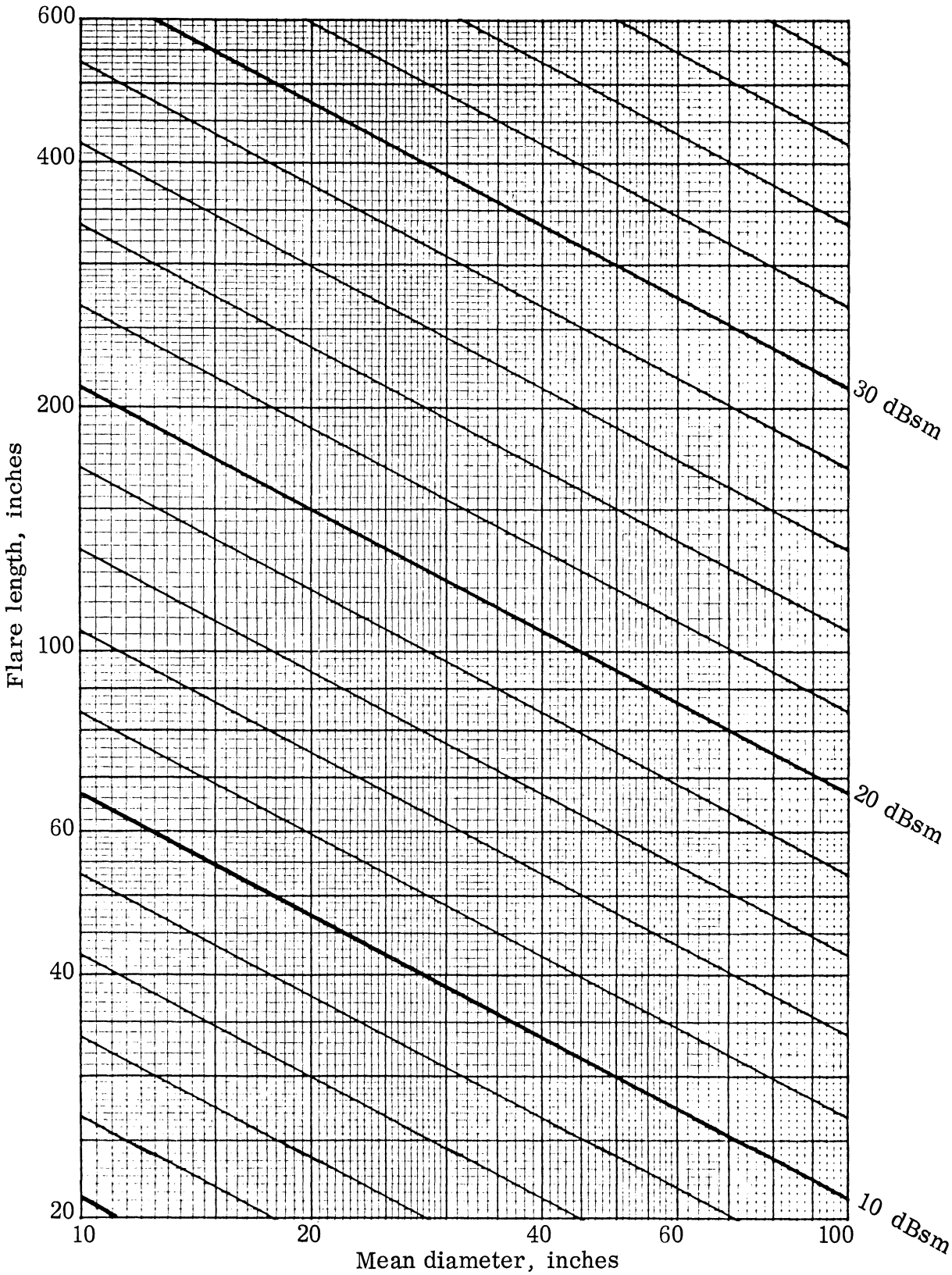

FIG. B-4: The specular radar return of a cylinder or cone frustum can be found from this L-band chart.

REFERENCES

Bechtel, M.E., "Application of Geometric Diffraction Theory to Scattering from Cones and Disks," Proc. IEEE, Vol. 53, pp. 877-882, 1965.

Bowman, J.J., "Comparison of Ray Theory with Exact Theory for Scattering by an Open Waveguide," IEEE Trans. Antennas and Propagation, Vol. AP-18, pp. 131-132, 1970.

Blore, W.E., "The Radar Cross Section of Ogives, Double-Backed Cones, Double-Rounded Cones, and Cone Spheres," IEEE Trans. Ant. and Prop. AP-12, pp. 582-590, 1964.

Flammer, C., "The Vector Wave Function Solution of the Diffraction of Electromagnetic Waves by Circular Disks and Apertures-II: The Diffraction Problems," J. Appl. Phys. Vol. 24, pp. 1224-1231, 1953.

Keller, J.B., "Backscattering From a Finite Cone," IRE Trans. Antennas and Propagation, AP-8, pp. 175-182, 1960.

Keys, J.E. and R.I. Primich, "The Radar Cross Section of Right Circular Metal Cones; I" Defense Research Telecommunications Establishment Report No. 1010.

Knott, E.F., A.G. Cole, K.M. Jagdmann and G.R. Mattson, "Analysis of Methods of Gathering and Interpreting ARIS Data," University of Michigan Radiation Laboratory Report No. 08798-4-T, (SECRET), 1969.

Knott, E.F., "Laboratory Method of Measuring the Phase of a Backscatter Signal," Institution of Electrical Engineers, Electronic Letters, Vol. 5, No. 25, pp. 667-668, 1969.

Knott, E.F., T.B.A. Senior and P.L.E. Uslenghi, "High-Frequency Backscattering from a Metallic Disk," submitted to IEEE Trans. AP, 1970.

Mattson, G.R., "Electromagnetic Plane Wave Scattering by a Perfectly Conducting Disk," Ph.D. Thesis, University of Michigan (1970a).

Mattson, G.R., "Backscattering from a Thin Metallic Disk," submitted to IEEE Trans. AP (Communication) (1970b).

Ross, R.A., "Investigation of Scattering Center Theory," Cornell Aeronautical Laboratory Technical Report No. AFAL-TR-67-343, December, 1967.

Ross, R.A., "Radar Cross Section of Rectangular Flat Plates as a Function of Aspect Angle," IEEE Trans. Antennas and Propagation, Vol. AP-14 pp. 329-335, 1966.

References, continued.

Ryan, C.E., Jr. and L. Peters, Jr., "Evaluation of Edge-Diffracted Fields Including Equivalent Currents for the Caustic Regions," IEEE Trans. Antennas and Propagation, AP-17, pp. 292-299, 1969.

Ryan, C.E., Jr., and L. Peters, Jr., "Correction to Evaluation of Edge Diffracted Fields Including Equivalent Currents for the Caustic Regions," IEEE Trans. Antennas and Propagation, AP-18, p. 275, 1970.

Senior, T.B.A., "Physical Optics Applied to Cone-Sphere-Like Objects," University of Michigan Radiation Laboratory Report No. 8525-2-T, 1967.

Stratton, J.A., P.M.Morse, L.J.Chu, J.D.C.Little and F.J.Corbaro, Spheroidal Wave Functions, John Wiley and Sons, Inc. 1956.

Ufimtsev, P. Ia., "Approximate Calculation of the Diffraction of Electromagnetic Waves by Certain Metal Ofjects-II: The Diffraction by a Disk and A Finite Cylinder," Soviet Phys.-Tech. Phys., Vol 3, pp. 2386-2396, 1958.

Weinstein, L.A., The Theory of Diffraction and the Factorization Method, The Golem Press, Boulder, Colorado, 1969.(Translated frmo Russian by P. Beckmann.)

UNCLASSIFIED

Security Classification

DOCUMENT CONTROL DATA - R & D

(Security classification of title, body of abstract and indexing annotation must be entered when the overall report is classified)

1. ORIGINATING ACTIVITY *(Corporate author)*
The University of Michigan Radiation Laboratory, Dept. of Electrical Engineering, 201 Catherine Street, Ann Arbor, Michigan 48108

2a. REPORT SECURITY CLASSIFICATION
UNCLASSIFIED

2b. GROUP

3. REPORT TITLE
ANALYSIS OF ARIS DATA

4. DESCRIPTIVE NOTES *(Type of report and inclusive dates)*
Final Report (1 December 1969 - 1 July 1970): Volume 1.

5. AUTHOR(S) *(First name, middle initial, last name)*
Eugene F. Knott and Thomas B. A. Senior

6. REPORT DATE	7a. TOTAL NO. OF PAGES	7b. NO. OF REFS
July 1970	82	19

8a. CONTRACT OR GRANT NO.	9a. ORIGINATOR'S REPORT NUMBER(S)
F08606-69-C-0045	2649-1-F, Vol. 1
b. PROJECT NO.	
c.	9b. OTHER REPORT NO(S) *(Any other numbers that may be assigned this report)*
d.	

10. DISTRIBUTION STATEMENT
Volume 2 of this Final Report is available from Air Force Eastern Test Range, Attn: ETEQO, Patrick AFB, Fla., 32925 upon approval from FTD, TDD, Wright-Patterson AFB, O. 45433.

11. SUPPLEMENTARY NOTES	12. SPONSORING MILITARY ACTIVITY
	Air Force Eastern Test Range ARIS Ships Re-entry Division Patrick Air Force Base, Florida 32925

13. ABSTRACT

In Volume 1 of this Final Report, we firstly touch on the major contributions made during the 38-month span of two successive contracts, which to all intents address a single goal: to assess the data and data collection techniques of the advanced range instrumentation ships, and to recommend how improvements could be made. The technical details of the report commence with a description of a final laboratory test of the five-parameter method conceived and described in the preceding report. The test suggested that polarization angle history can be a potential source of aspect angle information and this possibility is examined for the case of circular polarization. A summary of the extensive theoretical and experimental work on cone and disk scattering is given, showing how the disk results contributed to the more practical case of the cone. We conclude with a recommendation that the five-parameter method be seriously considered for instrumentation.

In Volume 2 of this Final Report, we present a sequence of three related test support missions and a comparison shows that differences as well as similarities exist.

DD FORM 1 NOV 68 1473

UNCLASSIFIED

Security Classification

14. KEY WORDS	LINK A		LINK B		LINK C	
	ROLE	WT	ROLE	WT	ROLE	WT
Radar Signature						
Radar Echoes						
Body Motion						
Re-entry Vehicle						
Sizing						
Multiple Polarizations						
Polarization Angle History						
Principal Plane Patterns						
Signature Analysis						
Five-Parameter Method						
Cone Scattering						
Disk Scattering						
Elliptical Precession						